

Supplemental Materials

Targeting macrophages for enhancing CD47 blockade-elicited lymphoma clearance and overcoming tumor-induced immunosuppression

Authors: Xu Cao¹, Yingyu Wang², Wencan Zhang³, Xiancai Zhong³, E. Gulsen Gunes^{1,4}, Jessica Dang¹, Jinhui Wang⁵, Alan L. Epstein⁶, Christiane Querfeld^{1,4,7,8}, Zuoming Sun³, Steven T. Rosen^{4,9#}, Mingye Feng^{1#}

Correspondence to: Steven T. Rosen, M.D., srosen@coh.org; Mingye Feng, Ph.D., mfeng@coh.org

Supplemental Methods

Flow cytometry and sorting

For flow cytometric analysis of *in vitro* cultured cancer cells or BMDMs, the following antibodies were used: anti-human CD47 (BD Biosciences), anti-human Calreticulin (Enzo Life Sciences), anti-mouse Sirp α (BioLegend), anti-mouse Calreticulin (ThermoFisher Scientific), anti-mouse Fc γ RI (BioLegend), anti-mouse Fc γ RIIB (BioLegend), anti-mouse Fc γ RIII (BioLegend), and anti-mouse Fc γ RIV (BioLegend). Analyses of mouse femur samples were performed using the following antibodies: anti-human CD19 (BD Biosciences), anti-mouse CD11b (BioLegend), anti-mouse F4/80 (BioLegend), and anti-human CD47 (BD Biosciences). Whenever the analysis was performed on samples containing macrophages, the samples were blocked with mouse Fc receptor blockers (Miltenyi) for 15 min on ice before staining with antibodies. For sorting femur macrophage, the single-cell suspension was prepared followed by ACK lysis to remove red blood cells. Subsequently, the Fc receptors on macrophages were blocked with a mouse Fc blocker and then the samples were stained with antibodies. The femur macrophages were defined as Sytox^hCD19⁻CD11b⁺F4/80⁺ cells.

Cell culture

Raji, SW480, DLD1, and A20 cell lines were obtained from ATCC. SU-DHL-1, SU-DHL-2, SU-DHL-5, and SU-DHL-7 cell lines were generated in Dr. Epstein's laboratory¹⁻⁶. Mac1 cell line was a generous gift from Dr. Marshall Kadin at Roger Williams Medical School. Daudi and Ramos cell lines were generous gifts from Dr. Jun Minowada at Roswell Park Memorial Institute. SW480 cells were cultured in DMEM supplemented with 10% (v/v) FBS and 1% penicillin (100 U)/streptomycin (100 mg/ml), and all the other cell lines were cultured in RPMI supplemented with 10% (v/v) FBS and 1% penicillin (100 U)/streptomycin (100 mg/ml). Cells were cultured in a humidified atmosphere of 95% and 5% CO₂ at 37°C. The cells were regularly screened to ensure no mycoplasma contamination.

Generation of macrophages

BMDMs were generated with six- to ten-week-old BALB/c mice. Specifically, bone marrow cells were flushed out with a 25 G needle from the femurs and filtered through a 70- μ m strainer. Upon pelleting the cells by centrifugation, red blood cells were lysed with ACK lysis buffer at room temperature for 2 min followed by washing with IMDM supplemented with 10% FBS. The cells were then cultured in IMDM containing 10% FBS and 10 ng/ul murine MCSF. BMDMs from day 6 to day 8 were used for functional assays in the work.

For human macrophages, monocytes were enriched from human peripheral blood by a magnetic-activated cell sorting method with whole blood CD14 microbeads (Miltenyi). CD14⁺ monocytes were then cultured in IMDM supplemented with 10% human serum. Human macrophages from day 6 to day 8 were used for this study.

Luminescence-based long-term macrophage killing assay (LB-LTMK)

Cancer cell lines such as Raji, Mac1, and A20 cells were transduced with a luciferase-eGFP fusion protein and used to set up the LB-LTMK assay. Specifically, cancer cells were co-cultured with macrophages for 24 h in IMDM supplemented with 10% FBS in the presence or absence of antibodies and/or drug treatment.

After incubation, luciferin was added into each well using a multichannel pipettor followed by detection of luminescence signal with Cytation 3. Cancer cells with corresponding drug treatment in the absence of macrophages were used as a normalization control for calculation, in which the phagocytosis rate was 0%. The phagocytosis rate was quantified as the ratio of signals in the treatment group to the signals cancer cells only.

LB-LTMK screen of 147 anti-cancer small molecules

The FDA-approved oncology drug library including 147 current approved anticancer small molecules was obtained from the Division of Cancer Treatment & Diagnosis at the National Cancer Institute (NCI) and used to identify potential enhancers of CD47 blockade. Specifically, individual drugs (10 μ M) from the library were incubated with 0.03×10^6 Raji cells expressing luciferase and 0.06×10^6 BMDMs in the absence or presence of CD47 blockades (aCD47 or aSirp α) in 96 well plates for 24 h. Subsequently, luciferin was added in the wells with a multiple-channel pipettor and luminescence signals were measured with Cytation 3. Wells containing 10 μ M drug and Raji cells without BMDMs were used as a normalization control for the calculation of phagocytosis rate. Drug sensitivity scores were calculated by normalizing the phagocytosis rate by individual drugs to phagocytosis rate by DMSO control.

Phagocytosis assay by flow cytometry or microscopy

Cancer cells were labeled with CellTrace Green. Briefly, 200 nM CellTrace Green in PBS was used to label cancer cells for around 20 min in the cell culture incubator (37°C). The cells were then washed with RPMI supplemented with 10% FBS followed by another wash with PBS. Macrophages cultured in Petri dishes were harvested by digestion with 0.05% trypsin for 3 min and cocultured with the prelabeled cancer cells in the presence or absence of CD47 blockades (anti-human CD47, BioXcell; anti-mouse CD47, BioXcell; anti-mouse Sirp α , BD Biosciences) for 2 h at 37°C. Before FACS, anti-F4/80 antibody (BioLegend) conjugated with PE-Cy7 was used to label macrophages. Phagocytosis was quantified as the percentage of macrophages that phagocytosed cancer cells during the incubation, namely the ratio of CellTrace Green⁺PE-Cy7⁺ cells to PE-Cy7⁺ cells. The phagocytosis index was normalized to the maximal response in every

experiment. For evaluating the efficacy of paclitaxel in phagocytosis assays, multiple NHL cell lines with different subtypes (Burkitt's Lymphoma, Large Cell Lymphoma and T cell Lymphoma), including the ones with different phospholipid scramblases expression and/or ability to present phosphatidylserine on the cell surface⁷⁻⁹, were used.

For fluorescent microscopic images of phagocytosis assays, sorted femur macrophages were placed in IMDM with 10% FBS in 24-well tissue culture plates overnight. The cells were then stained with CellTrace Green for 10 minutes at 37°C followed by washing with the medium. Fresh IMDM with 10% FBS was then added. Target cancer cells i.g. Raji cells were stained with pHrodo™ Red at a final concentration of 120 ng/ml for 15 minutes. The cells were then washed one with RPMI supplemented with 10% FBS followed by another wash with PBS. Next, target cancer cells were cocultured with BMDMs for 8 hours with or without aCD47. The fluorescence image was taken under a fluorescence scope (Leica).

CRISPR editing

CD47 knockdown cells were generated with CRISPR/Cas9 system followed by FACS sorting. Specifically, Pairs of primers containing sequences of control sgRNA (GAACGUAGAAAUCCCAUUU)¹⁰ or sgRNA targeting human CD47 (CUACUGAAGUAUACGUAAAG)¹⁰ were designed and cloned into the all-in-one LentiCRISPR V2 vector¹⁰. LentiCRISPR v2 was a gift from Feng Zhang (Addgene plasmid #52961). Viruses were generated by transfecting the LentiCRISPR V2 vector with the packing plasmid into HEK293T cells and stored at -80°C after filtering through a 0.45 µm strainer. For the infection, Raji cells were incubated with the corresponding viruses for 48 h in the presence of 8 µg/ml polybrene and selected with puromycin (2 µg/ml) after the removal of the virus. FACS sorting was then employed to make sure the complete absence of CD47 expression on these cells.

Cell viability assay

Cancer cells (Raji or Daudi cells) subjected to various treatments were collected and washed with PBS. Subsequently, the cells were stained with Annexin V-APC (BioLegend) and Sytox blue (ThermoFisher) at

room temperature for 10 min followed by analysis with flow cytometry. Viable cells were defined as Annexin V⁻/Sytox blue⁻ populations.

Mouse and therapeutics

For the evaluation of drug efficacy on the systemic NHL disease model, 3×10^6 Raji cells expressing a luciferase-eGFP fusion protein were intravenously injected into RAG2^{-/-}γc^{-/-} BALB/c mice. Nab-paclitaxel was obtained from the City of Hope Helford Research Hospital and used for intravenous injection. Either nab-paclitaxel or aCD47 was given intravenously at doses and time periods as specified in each figure. For the evaluation of local effects of paclitaxel on CD47 antibody, 0.5 M Raji or A20 cells expressing a luciferase-eGFP fusion protein or 1 M Daudi or SU-DHL-2 cells were subcutaneously planted on RAG2^{-/-}γc^{-/-} BALB/c mice or BALB/c mice. For the Raji, Daudi, or SU-DHL-2 tumors, treatment was started on day 20 after engraftment by intratumoral injection of 2 ug paclitaxel and intravenous injection of aCD47 (100 μg/mouse; clone B6H12 (mouse IgG1), BioXCell) twice every week for three weeks. For the A20 tumors, treatment was started on day 5 after engraftment by co-injection of 2 ug paclitaxel and aCD47 (50 μg/tumor; clone MIAP410 (mouse IgG1), BioXCell) weekly for a total of three weeks. Tumor progression was regularly monitored by bioluminescence imaging (Raji and A20) or measurement of tumor volume (Daudi and SU-DHL-2).

Gene knockdown by siRNA in primary macrophages

The siRNA knockdown of genes from primary BMDMs was performed with siGENOME SMARTpool from Dharmacon™ in 96 well plates. Specifically, siScramble or siRNA of target genes was incubated with transfection reagent DharmaFECT4 for 30 min followed by the addition of primary BMDMs. Each well contained 0.06 M BMDMs together with 50 nM siRNA and 0.6 ul DharmaFECT4. After 48 h incubation, the medium was replaced with fresh IMDM with 10% of FBS followed by LB-LTMK assay to evaluate the phagocytosis ability of the macrophages as described in the figure legend.

Bioluminescence imaging

Tumor progression was routinely monitored by bioluminescent imaging on a Lago X instrument (Spectral Instruments Imaging). Mice were intraperitoneally injected with D-luciferin (140mg/kg; Biosynth Carbosynth) and then anesthetized by 2 to 3% isoflurane inhalation. Mice were imaged inside the camera box with continuous exposure to isoflurane. Data were analyzed with Aura software (Spectral Instruments Imaging) where regions of interest were drawn and quantified as photons per second.

In vivo depletion of macrophages

Macrophages were depleted *in vivo* through intravenous injection of liposome-encapsulated clodronate. Mice were given either clodronate-liposome or PBS-liposome (200 ul) every other day for a total of two injections; The combination treatment of paclitaxel (given at day10) and aCD47 (given at day11) was given to the mice. Forty-eight hours after the final injection of clodronate, mice were subject to bioluminescence imaging to evaluate the effect of macrophage depletion on the treatment efficacy. Subsequently, femur macrophage depletion was verified by flow cytometry analysis, and femur macrophages were defined as Sytox⁻hCD19⁻CD11b⁺F4/80⁺ cells. The effect of clodronate on TAM depletion and lymphoma growth was quantified for each femur.

Bulk RNA sequencing of femur macrophages

RNA of sorted femur macrophages (CD11b⁺F4/80⁺) were extracted with an RNA extraction kit (Qiagen). The samples were submitted to Novogene Inc. for library preparation and subsequent RNA sequencing. RNA was used for cDNA library construction using a NEBNext® Ultra RNA Library Prep Kit for Illumina® (New England Biolabs) according to the manufacturer's protocol. The resulting 250-350 bp insert libraries were quantified using a Qubit 2.0 fluorometer (Thermo Fisher Scientific) and quantitative PCR. Size distribution was analyzed using an Agilent 2100 Bioanalyzer (Agilent Technologies). Qualified libraries were sequenced on an Illumina HiSeq 4000 Platform (Illumina) using a paired-end 150 run (2×150 bases). Reads containing adapter or poly-N and those of low quality were trimmed after which gene counts were obtained through mapping the clean reads to reference genome mm10 using STAR 2.5.3a. The counts were then normalized into fragments per kilobase of transcript per million reads (FPKM) which was used

as the original raw data and analyzed by GSA algorithm to find differentially expressed genes (Fig.5C). In the volcano plots (Fig.5A, Fig.5B and Fig.S5A) and comparison with single-cell RNA sequencing (Fig.6B), the bulk RNAseq data were aligned to mm10 mouse genome (GENCODE vM23/Ensembl 98)) with STAR(v.2.5.3a) on the PartekFlow platform, normalized into Count per Million then log transformed. The GSA algorithm was applied to find 405 differentially expressed genes (fold change FC >2 and p value<0.05) from a total of 17528 genes.

Single-cell RNA sequencing

RAG2^{-/-}γc^{-/-} BALB/c mice were engrafted with Raji cells and treated with control vehicle, aCD47, nab-paclitaxel, or a combination of aCD47 and nab-paclitaxel starting at day 11 after engraftment. CD11b⁺ myeloid cells were sorted from the bone marrow of the mice and RNA of sorted cells were extracted with an RNA extraction kit (Qiagen). The samples were submitted to Integrative Genomics Core at City of Hope for library preparation and subsequent RNA sequencing.

Around 3,000 cells were captured per sample on a 10xGenomics Chromium controller using a 10X V3.1 Single Cell 3' Solution kit (10xGenomics, Chromium Next GEM Single Cell 3' Reagent kits V3.1). All protocols were performed following the manufacture's instruction. Final sequencing libraries were analyzed on a High Sensitivity DNA Chip (Agilent Technologies) to determine the library size. The library concentration was determined with a Qubit High Sensitivity DNA assay Kit (ThermoFisher Scientific). The libraries were sequenced with the paired-end setting of 28 cycles of read1, 101 cycles of R2, 8 cycles of index i7 and 8 cycles of index i5 read on Illumina NovaSeq 6000 platform with S4 Reagent kit v1.5 (Illumina) at The Translational Genomics Research Institute (TGen).

Single-cell RNA-seq reads were quantified by Cell Ranger-5.0.0, aligned to mm10 mouse genome (GENCODE vM23/Ensembl 98). Each sample yielded >250 million aligned reads and > 95% percentage of aligned reads. Combined raw data from the four samples were filtered to remove cells that expressed fewer than 500 genes, or more than 6000 genes, or >10% mitochondrial reads, then normalized and log-transformed using the NormalizeData function from Seurat (v4.0.3). From 13588 sequenced cells, 12795

cells passed quality control with an expression of a total of 16740 genes. Top 2000 highly variable genes were identified using the Seurat vst algorithm. After scaling the data, running jackstraw, the elbow plot of standard deviation in each PC suggested the first 15 PCs captured the majority of true signals, which were used to generate the KNN neighborhood graph, and clustering was performed using the Louvain algorithm with 0.8 resolution.

Clusters 5,7,13,15,16,18 were separated based on the expression of TAM macrophage markers. Two further clustering methods were applied. 1) Unbiased clustering was performed by another iteration of scaling, variable genes and PCs identification (top 1000 genes and first 15 PCs), k-nearest neighbor graph generation and clustering with 0.4 resolution. Differentially expressed genes for each cluster were calculated using the Wilcoxon rank-sum test. 2) Supervised clustering was performed using 405 differentially expressed genes of bulk RNAseq between Day0/4 and Day18, and the first 10 PCs.

Western blot

After treatment, cells were washed twice with ice-cold PBS and lysed with RIPA buffer containing phosphatase and protease inhibitors. Protein concentration was measured with a BCA colorimetric kit. An equal amount of proteins from each sample was separated with sodium dodecyl sulfate-polyacrylamide gel electrophoresis (SDS-PAGE) and transferred onto a Nitrocellulose Membrane. After blocking with 10% nonfat milk, the membranes were incubated with a primary antibody overnight with mild shaking at 4°C. Then, the membrane was washed with TBST buffer and then incubated with a horseradish peroxidase-conjugated secondary antibody for 1 h at room temperature. The immunoblots were visualized with enhanced chemiluminescence (ECL) western blotting substrate. The membrane was stripped for other protein detection when necessary.

Analysis of clinical datasets

For analysis of immune cell composition in NHL patient specimens, the gene expression dataset GSE181063 was obtained from Gene Expression Omnibus (GEO). Gene expression profiling was

performed on RNA from Diffuse Large B Cell Lymphoma (DLBCL) patient specimens using the Illumina DASL platform. The Gene expression dataset was analyzed by using the bioinformatics analytical tool CIBERSORT which has been demonstrated to be highly concordant with ground truth cell proportions and gene expression profiles. CIBERSORT was used to impute immune cell fractions and cell-type-specific gene expression profiles. The LM22 gene expression matrix was employed, which can distinguish 22 hematopoietic cell types, and cell-type-specific gene expression analysis was based on merged 10 major immune cell types.

Supplemental Figures

Supplemental Figure 1: **A.** Bioluminescence imaging of mice engrafted with Raji cells through tail vein injection showing the dissemination of tumor cells into the bone marrow compartment and progression. Left: representative images; Right: quantified tumor signals; $***P < 0.001$ (one-way ANOVA test). **B.** Antibody infiltration experiment showing Raji cells (hCD19+) obtained from the bone marrow compartment was bound with aCD47. aCD47 was given on day 11 and day 16 post Raji engraftment through tail vein injection. 3 hours later, bone marrow cells were collected and stained for hCD19. **C.** Ratios of Raji or TAMs to the total live cells in the bone marrow at 4, 11, or 14 days after engraftment of RAG2^{-/-}γc^{-/-} mice with Raji cells; $***P < 0.001$ (t-test). **D.** Raji cells obtained from Raji engrafted mice (day 11) showed no difference to *in vitro* cultured counterparts in the susceptibility to BMDM phagocytosis in the presence of aCD47. **E.** Sorting strategy to obtain femur macrophages from Raji-engrafted mice.

Supplemental Figure 2: **A.** A schematic showing the experimental design of the LB-LTMK assay. **B.** A luminescence image showing CD47 blockades dose-dependently eliminates various tumor cells in an LB-LTMK assay. **C.** A comparison of the accuracy of phagocytosis rates obtained by quantifying the GFP signals from surviving cancer cells to those obtained by quantifying surviving cells with flow cytometry (standard method). **D.** A comparison of the accuracy of phagocytosis rates obtained by quantifying the luminescence signals from surviving cancer cells to those obtained by quantifying surviving cells with flow cytometry (standard method). In (C) and (D), human cancer lines SW480, DLD1, and Raji were used. **E.** Phagocytosis rates obtained from independent experiments with aSirpα showing the excellent accuracy LB-LTMK assay in determining long-term phagocytosis rates. **F.** The correlation of phagocytosis changes between screens with anti-CD47 and anti-Sirpα antibodies; Spots represent individual compounds.

Supplemental Figure 3: **A.** Representative FACS plots showing the expression of CD47 on Ctrl^{KD} and CD47^{KD} Raji cells. **B.** Paclitaxel significantly enhanced aCD47-mediated clearance of multiple NHL cell lines (Raji, Daudi, Ramos, SU-DHL-1, SU-DHL-2, SU-DHL-5, SU-DHL-7, Mac1 and A20); $**P < 0.01$,

*** $P < 0.001$ (t-test). **C-D**. Paclitaxel (5 μ M) or conditioned media from paclitaxel-treated BMDMs induced minimal cell death of Raji (**C**) or Daudi (**D**) cells. **E-F**. Co-culture with paclitaxel-treated BMDMs induced minimal cell death of Raji (**E**) or Daudi (**F**) cells; Cell viability of Raji or Daudi cells was analyzed at 0, 2, 8, or 20 hours of co-culture with BMDMs.

Supplemental Figure 4: A. Paclitaxel potentiated the effect of rituximab-mediated phagocytosis in a dose-dependent manner; *** $P < 0.01$ (one-way ANOVA test); rituximab was used at 10 μ g/ml. **B**. Pretreatment of BMDMs but not Raji cells with paclitaxel significantly enhanced rituximab-mediated phagocytosis; *** $P < 0.01$ (one-way ANOVA test); rituximab was used at 10 μ g/ml. **C**. Paclitaxel enhanced the potency and maximal capacity of rituximab for macrophage-mediated clearance of Raji cells. **D**. A phagocytosis assay showing rituximab induced phagocytosis of Raji cells but not CD20 deficient NHL cells (SU-DHL-1 and Mac1); Paclitaxel treatment of macrophages enhanced phagocytosis; *** $P < 0.001$ (t-test); rituximab was used at 10 μ g/ml. **E**. Paclitaxel significantly enhanced rituximab-mediated clearance of multiple human NHL cell lines (Daudi, Ramos, SU-DHL-2, SU-DHL-5, SU-DHL-7); *** $P < 0.001$ (t-test); rituximab was used at 10 μ g/ml.

Supplemental Figure 5: A-B. Expression of Sirp α (**A**) and calreticulin (**B**) on BMDMs after stimulating with paclitaxel overnight, as examined by FACS analysis. **C**. Expression of Fc γ RI, Fc γ RIIB, Fc γ RIII and Fc γ RIV on BMDMs after stimulating with paclitaxel overnight, as examined by FACS analysis.

Supplemental Figure 6: A. Representative animal images of mice from Fig3B showing the remarkable inhibitory effect of combining paclitaxel and aCD47 on tumor cell growth in RAG2^{-/-} γ c^{-/-} mice. **B**. and **C**. Growth of tumors derived from Daudi (**B**) and SU-DHL-2 (**C**) cells in RAG2^{-/-} γ c^{-/-} mice. Mice subcutaneously engrafted with Daudi cells or SU-DHL-2 cells were treated with control vehicle, aCD47, paclitaxel, or a combination of aCD47 and paclitaxel; Tumor growth was monitored by the measurement of tumor volume; *** $P < 0.001$ (log-linear regression analysis). **D-F**. Paclitaxel and nab-paclitaxel demonstrated similar effects on enhancing CD47-blockade-induced phagocytosis (**D**) and direct cytotoxicity toward Raji (**E**) and Daudi (**F**) cells; *** $P < 0.001$ (one-way ANOVA test). **G**. Representative FACS images showing the depletion of femur macrophage from mice bearing system Raji disease. **H**. Depletion efficiency of clodronate liposome on femur macrophages; *** $P < 0.001$ (t-test). **I**. Representative animal images of mice from Fig.3F showing that depletion of macrophages abolished the therapeutic effect of the combination in RAG2^{-/-} γ c^{-/-} mice.

Supplemental Figure 7: A. Volcano plots showing the comparison of differential gene expression of bone marrow macrophages from Raji-engrafted RAG2^{-/-} γ c^{-/-} mice at day0 (normal) and day18 (late) of engraftment. **B**. UMAP plots of scRNAseq of bone marrow CD11b⁺ cells from Raji-engrafted RAG2^{-/-} γ c^{-/-} mice treated with control vehicle, aCD47, nab-paclitaxel, or a combination of aCD47 and nab-paclitaxel. **C**. Percentage of cells in clusters 0 – 8 analyzed in (**B**). **D**. UMAP plots of scRNAseq of BM CD11b⁺ cells from Raji-engrafted RAG2^{-/-} γ c^{-/-} mice showing the expression of *Adgre1*, *Csf1r*, and *CD68* in subpopulations of CD11b⁺ cells.

Supplemental Figure 8: A. siRNA mediated knockdown of Btk or Src, but not Abl or Braf, compromised aCD47 mediated phagocytosis of Raji cells. B. Pretreatment with specific Src kinase inhibitor PP1 blunted paclitaxel-induced increase of macrophage phagocytic ability; *** $P < 0.001$ (one-way ANOVA test).

Supplemental Figure 9: A. Immune cell composition of a cohort of stage I – IV DLBCL patient biopsies, inferred by CIBERSORT; For biopsies with stages I, II, III, and IV, $n = 174, 213, 262,$ and 429 . B. – K. Expression of genes *Socs3*, *Sdc4*, *Mmp14* and *Arg2* in immune cells of stage I – IV DLBCL patient biopsies in (A), including macrophages (B), B cells (C), Plasma cells (D), CD8 T cells (E), CD4 T cells (F), $\gamma\delta$ T cells (G), NK cells (H), Dendritic cells (I), Mast cells (J) and Polymorphonuclear cells (K).

Supplemental Table 1: FDA-approved anticancer small molecule compounds for the LB-LTMK screening.

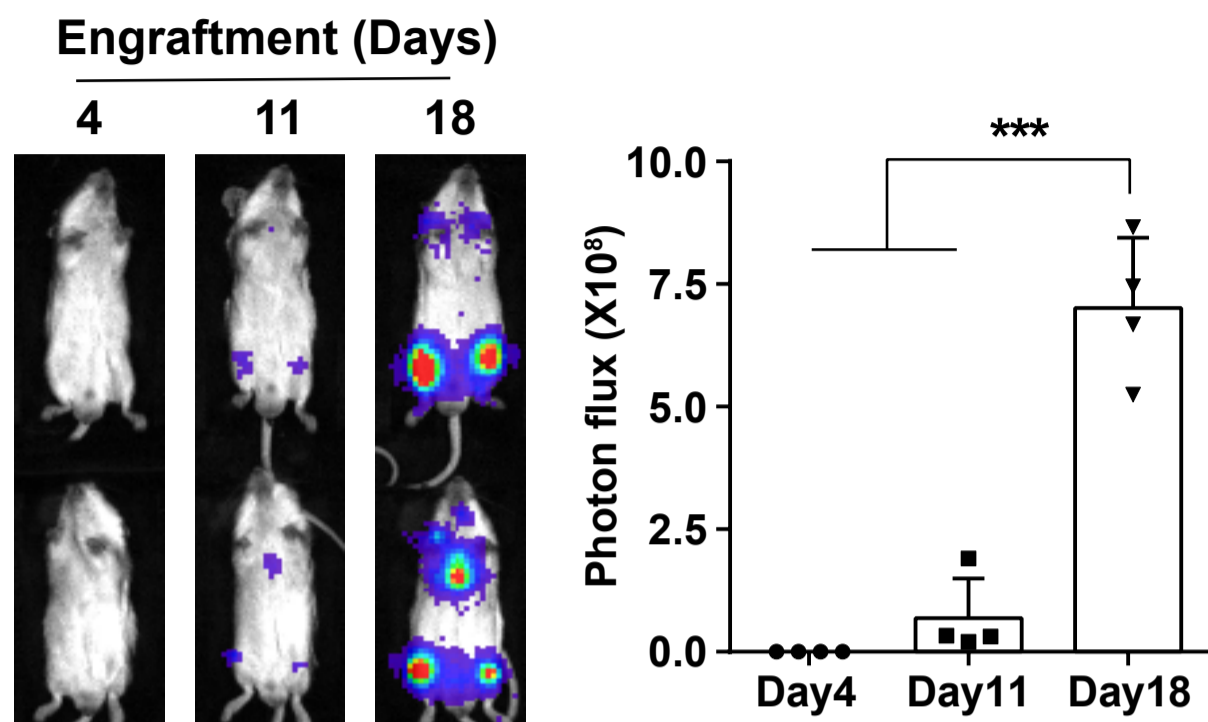
References

- 1 Epstein, A. L., Henle, W., Henle, G., Hewetson, J. F. & Kaplan, H. S. Surface marker characteristics and Epstein-Barr virus studies of two established North American Burkitt's lymphoma cell lines. *Proc. Natl. Acad. Sci. U. S. A.* **73**, 228-232, doi:10.1073/pnas.73.1.228 (1976).
- 2 Epstein, A. L. & Kaplan, H. S. Biology of the human malignant lymphomas. I. Establishment in continuous cell culture and heterotransplantation of diffuse histiocytic lymphomas. *Cancer* **34**, 1851-1872, doi:10.1002/1097-0142(197412)34:6<1851::aid-cnrc2820340602>3.0.co;2-4 (1974).
- 3 Epstein, A. L., Variakojis, D., Berger, C. & Hecht, B. K. Use of novel chemical supplements in the establishment of three human malignant lymphoma cell lines (NU-DHL-1, NU-DUL-1, and NU-AMB-1) with chromosome 14 translocations. *Int. J. Cancer* **35**, 619-627, doi:10.1002/ijc.2910350509 (1985).
- 4 Hecht, B. K., Epstein, A. L., Berger, C. S., Kaplan, H. S. & Hecht, F. Histiocytic lymphoma cell lines: immunologic and cytogenetic studies. *Cancer Genet. Cytogenet.* **14**, 205-218, doi:10.1016/0165-4608(85)90186-4 (1985).
- 5 Siminovitch, K. A., Jensen, J. P., Epstein, A. L. & Korsmeyer, S. J. Immunoglobulin gene rearrangements and expression in diffuse histiocytic lymphomas reveal cellular lineage, molecular defects, and sites of chromosomal translocation. *Blood* **67**, 391-397 (1986).
- 6 Winter, J. N., Variakojis, D. & Epstein, A. L. Phenotypic analysis of established diffuse histiocytic lymphoma cell lines utilizing monoclonal antibodies and cytochemical techniques. *Blood* **63**, 140-146 (1984).
- 7 Zhao, J., Zhou, Q., Wiedmer, T. & Sims, P. J. Level of expression of phospholipid scramblase regulates induced movement of phosphatidylserine to the cell surface. *J. Biol. Chem.* **273**, 6603-6606, doi:10.1074/jbc.273.12.6603 (1998).

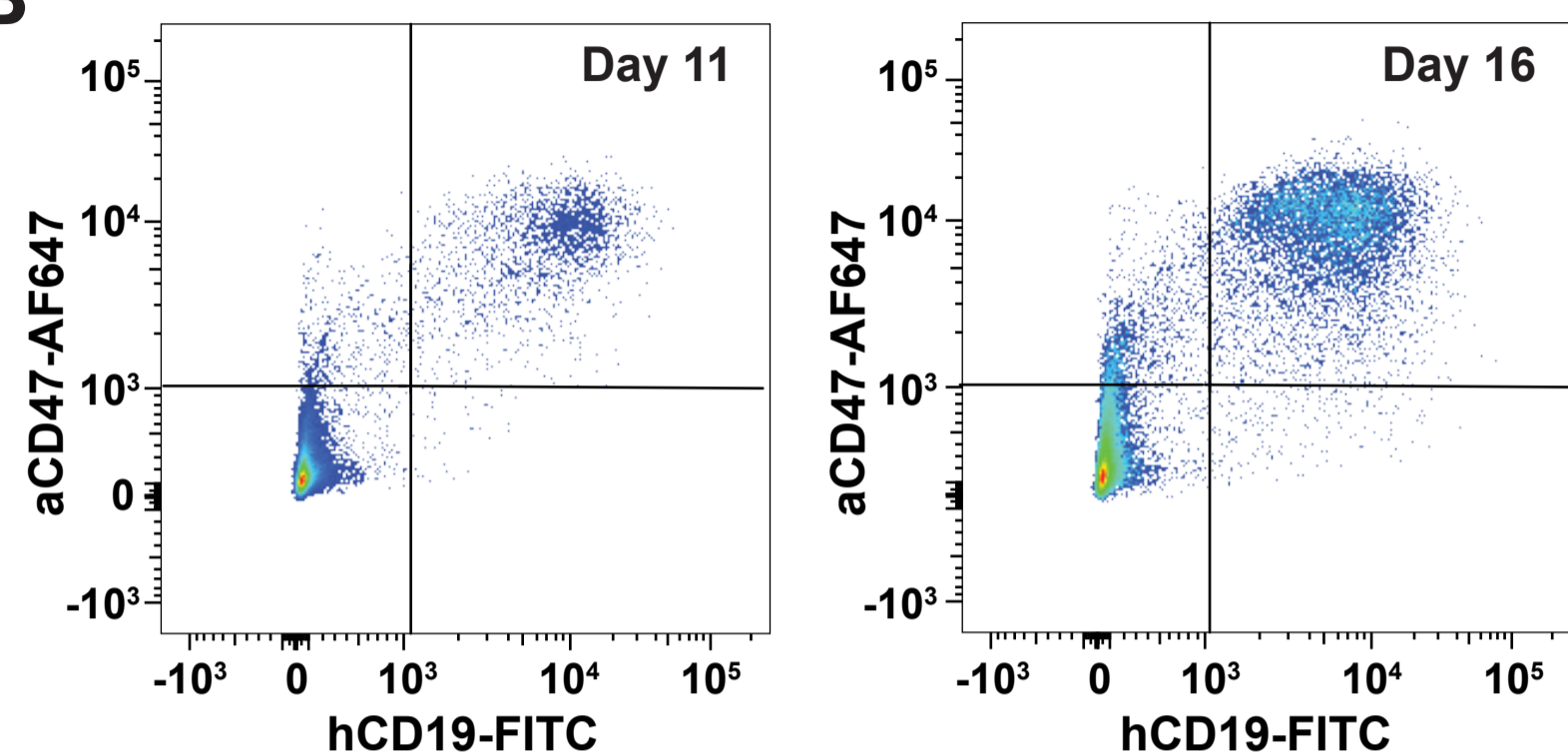
- 8 Kusano, S. & Ikeda, M. Interaction of phospholipid scramblase 1 with the Epstein-Barr virus protein BZLF1 represses BZLF1-mediated lytic gene transcription. *J. Biol. Chem.* **294**, 15104-15116, doi:10.1074/jbc.RA119.008193 (2019).
- 9 Chung, J. *et al.* Protein arginine methyltransferase 5 (PRMT5) inhibition induces lymphoma cell death through reactivation of the retinoblastoma tumor suppressor pathway and polycomb repressor complex 2 (PRC2) silencing. *J. Biol. Chem.* **288**, 35534-35547, doi:10.1074/jbc.M113.510669 (2013).
- 10 Sanjana, N. E., Shalem, O. & Zhang, F. Improved vectors and genome-wide libraries for CRISPR screening. *Nat Methods* **11**, 783-784, doi:10.1038/nmeth.3047 (2014).
- 11 Newman, A. M. *et al.* Robust enumeration of cell subsets from tissue expression profiles. *Nat Methods* **12**, 453-457, doi:10.1038/nmeth.3337 (2015).
- 12 Newman, A. M. *et al.* Determining cell type abundance and expression from bulk tissues with digital cytometry. *Nat Biotechnol* **37**, 773-782, doi:10.1038/s41587-019-0114-2 (2019).

Supplemental Figure 1

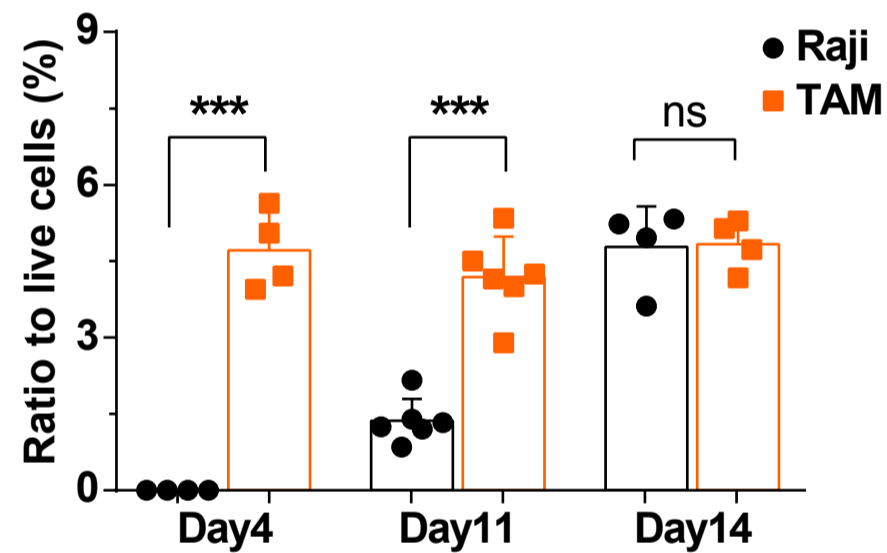
A



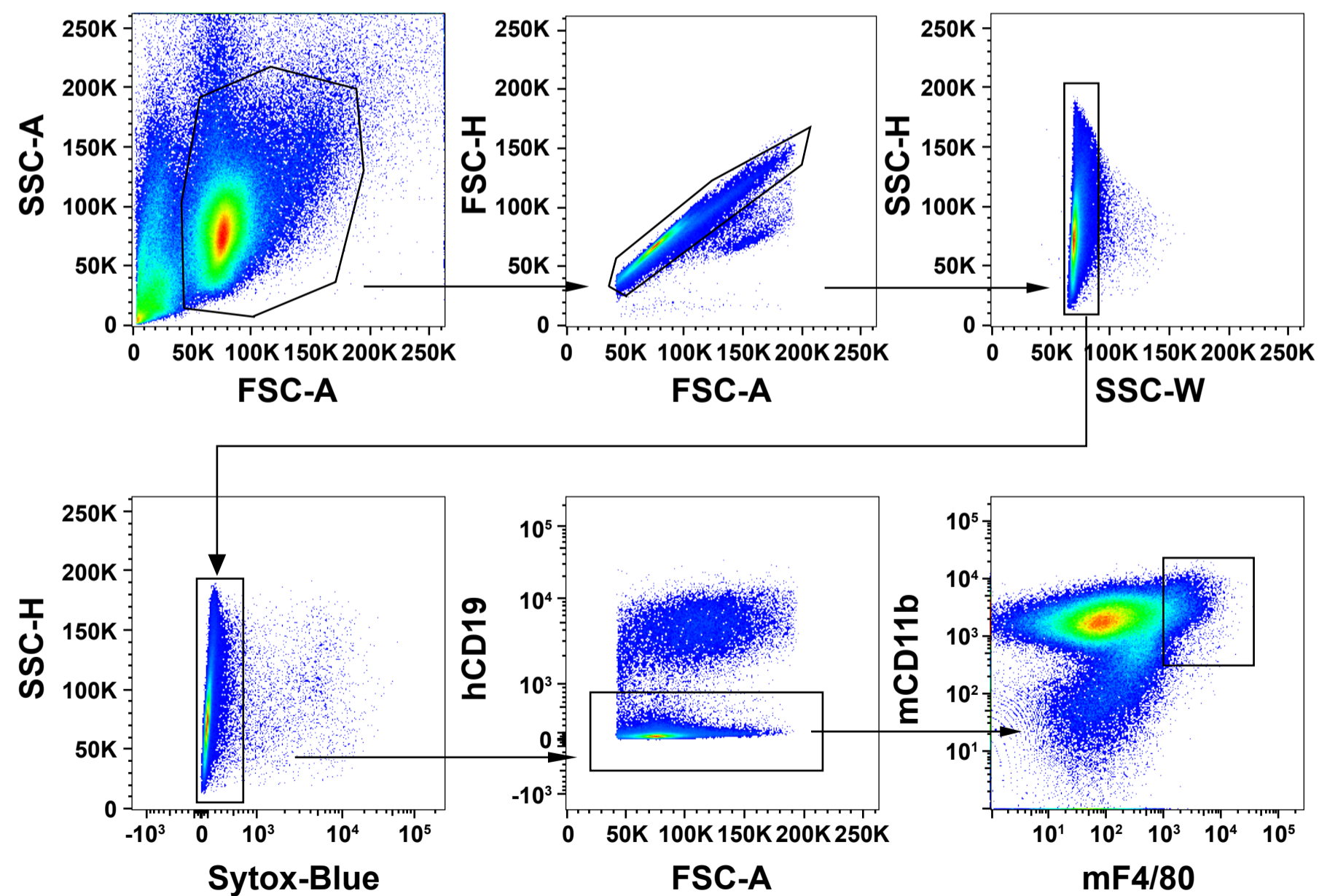
B



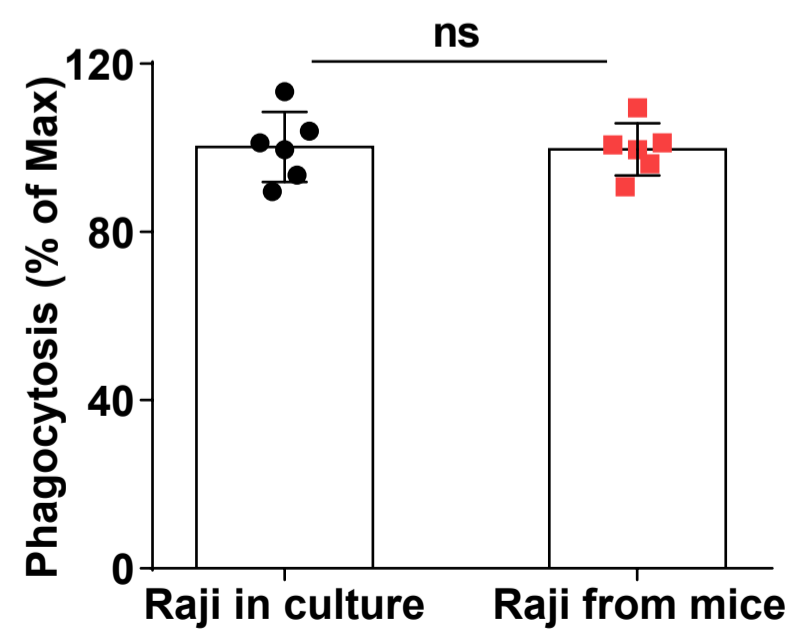
C



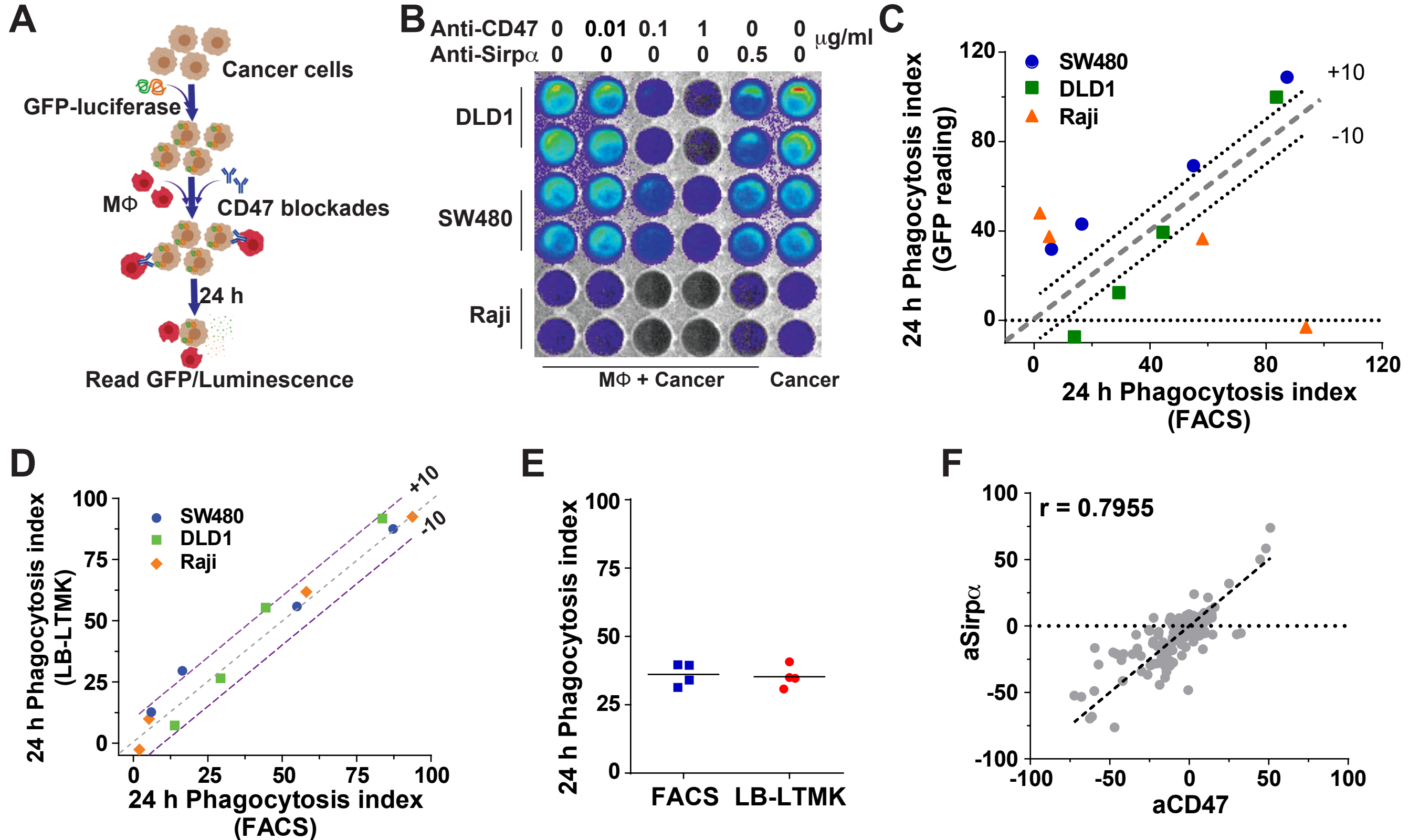
E



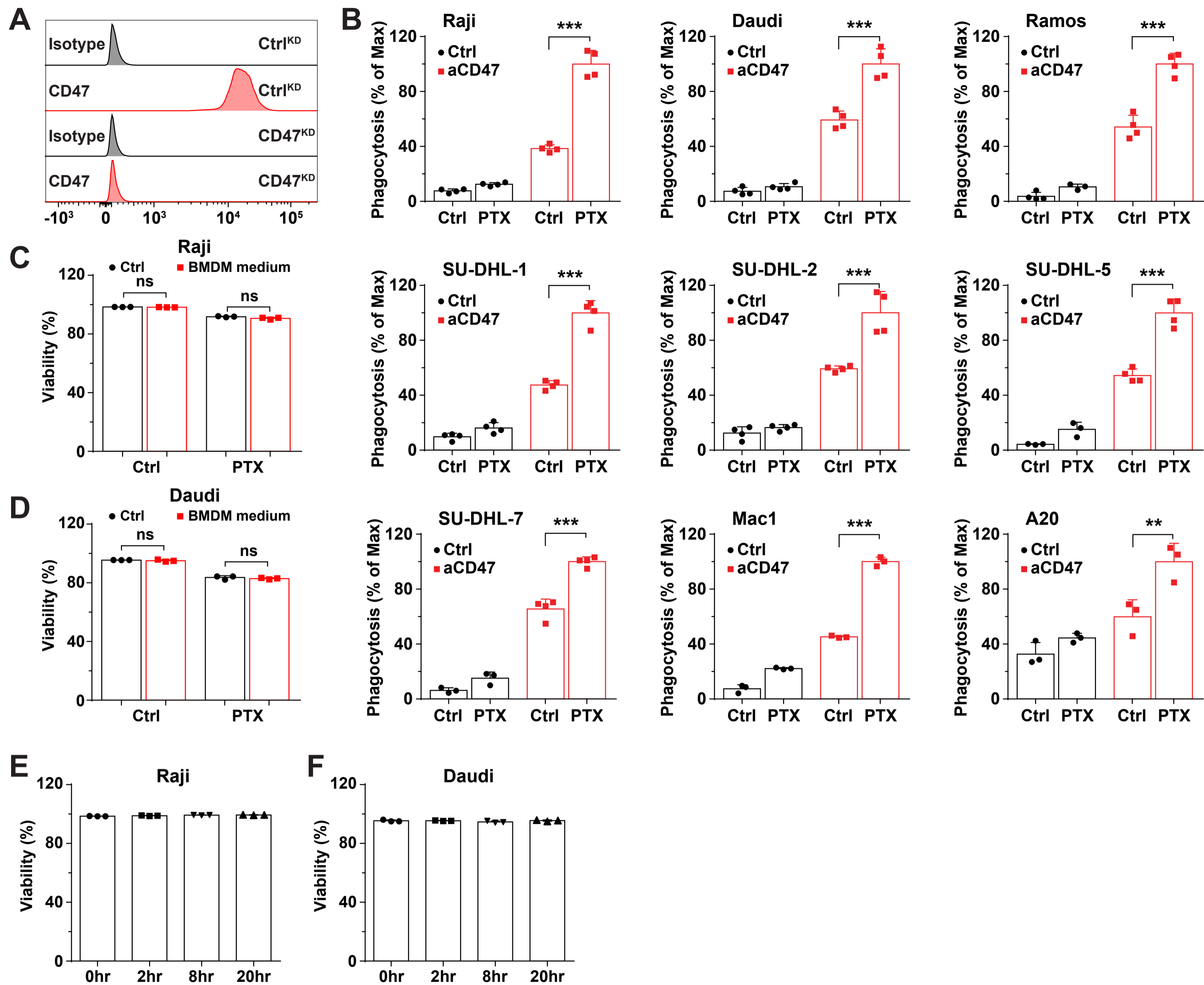
D



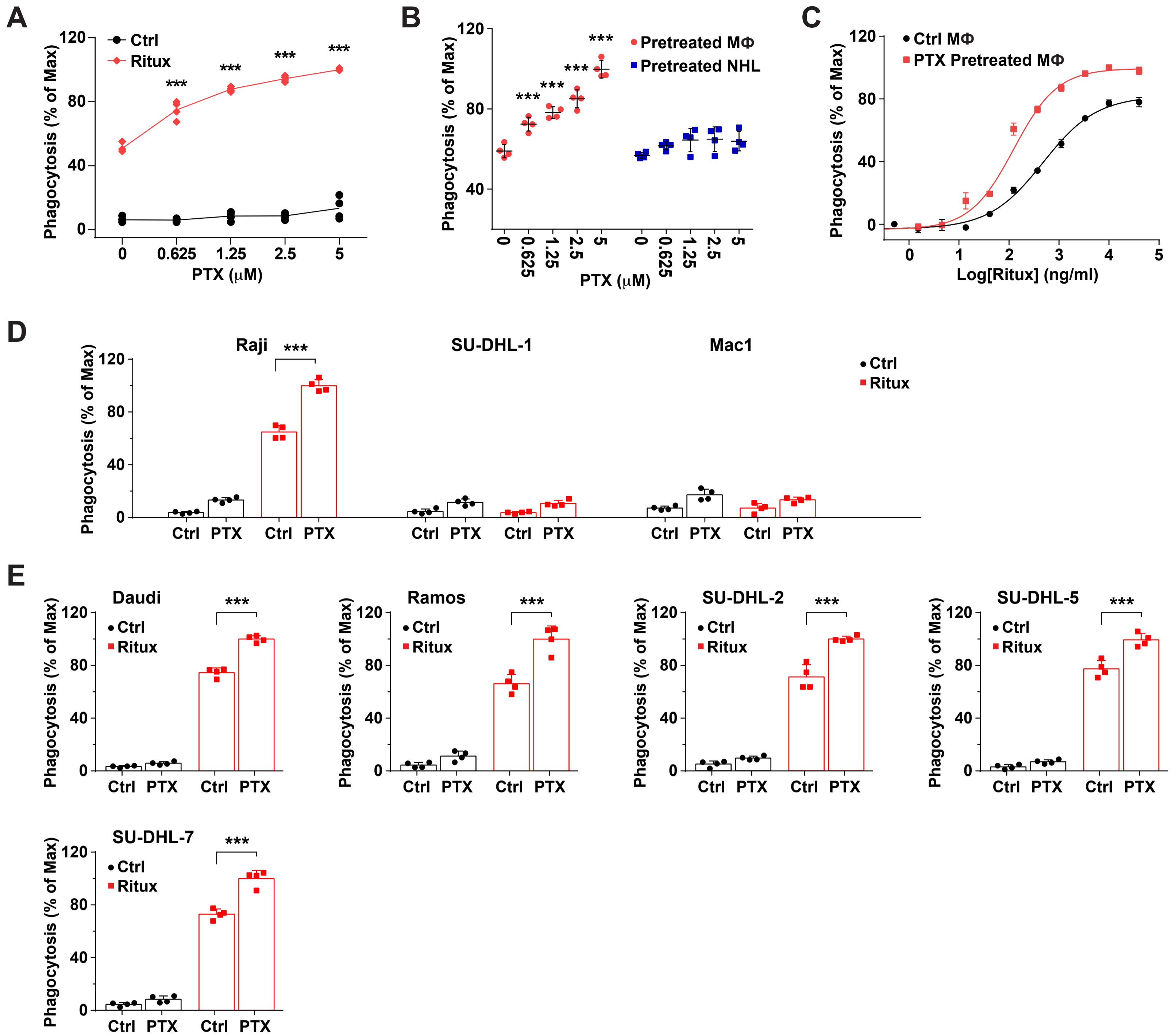
Supplemental Figure 2



Supplemental Figure 3

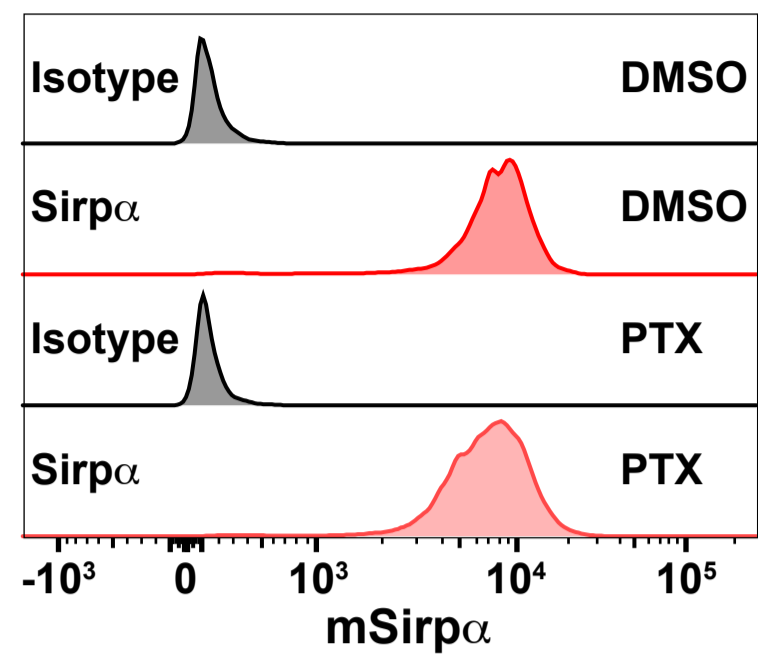


Supplemental Figure 4

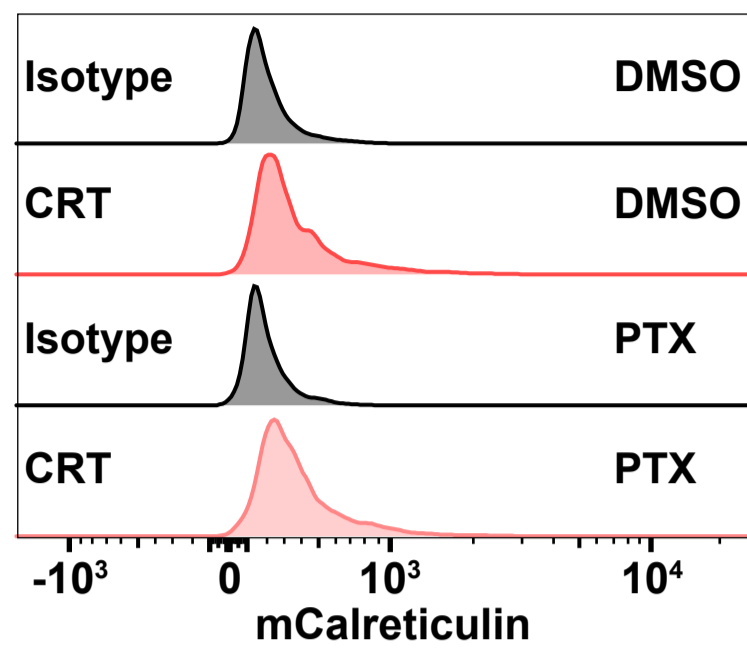


Supplemental Figure 5

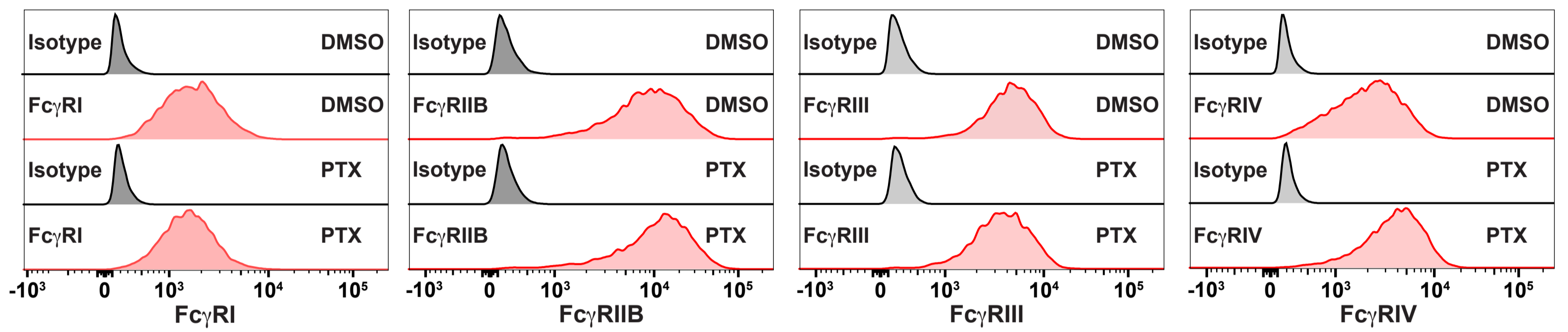
A



B

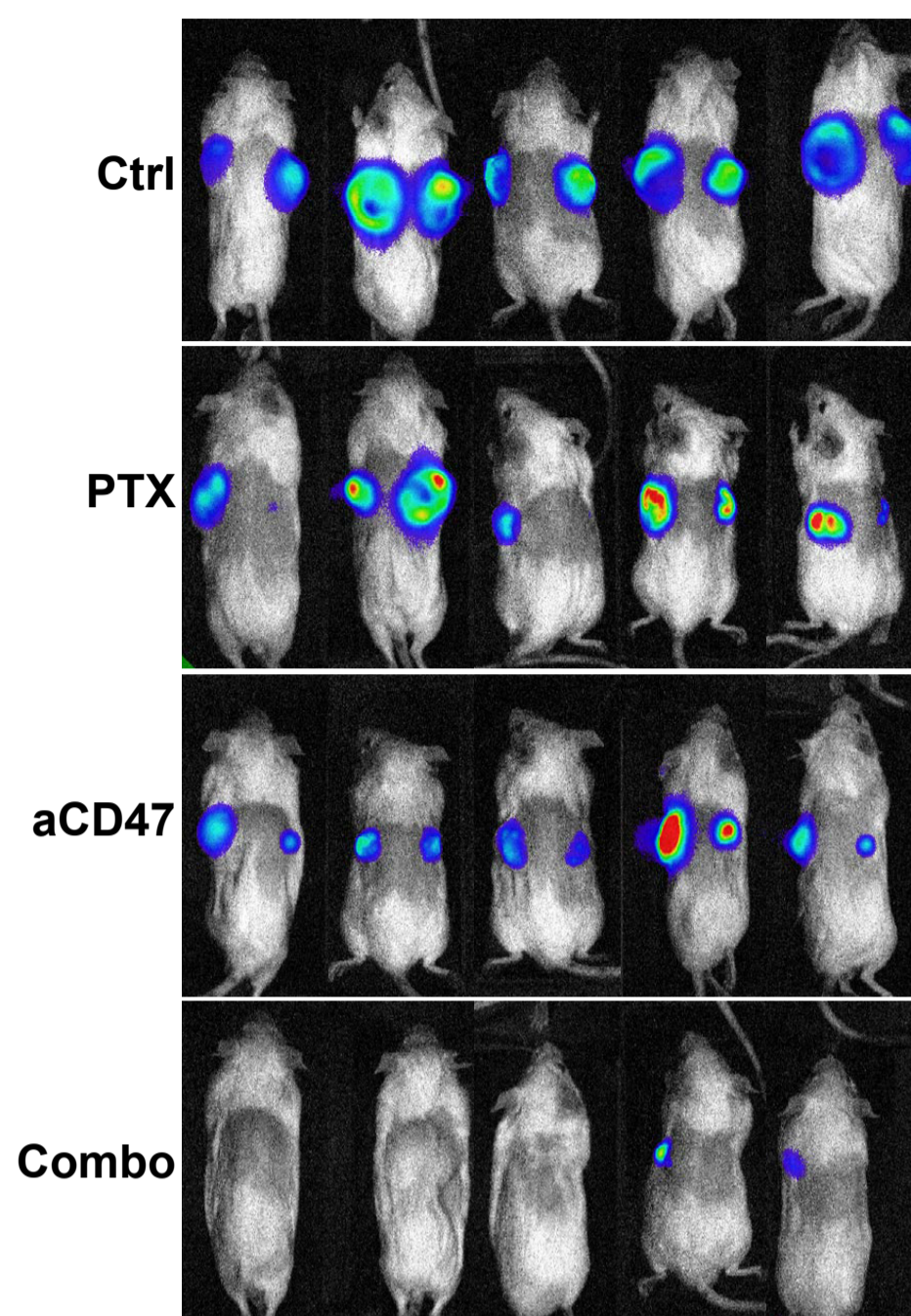


C

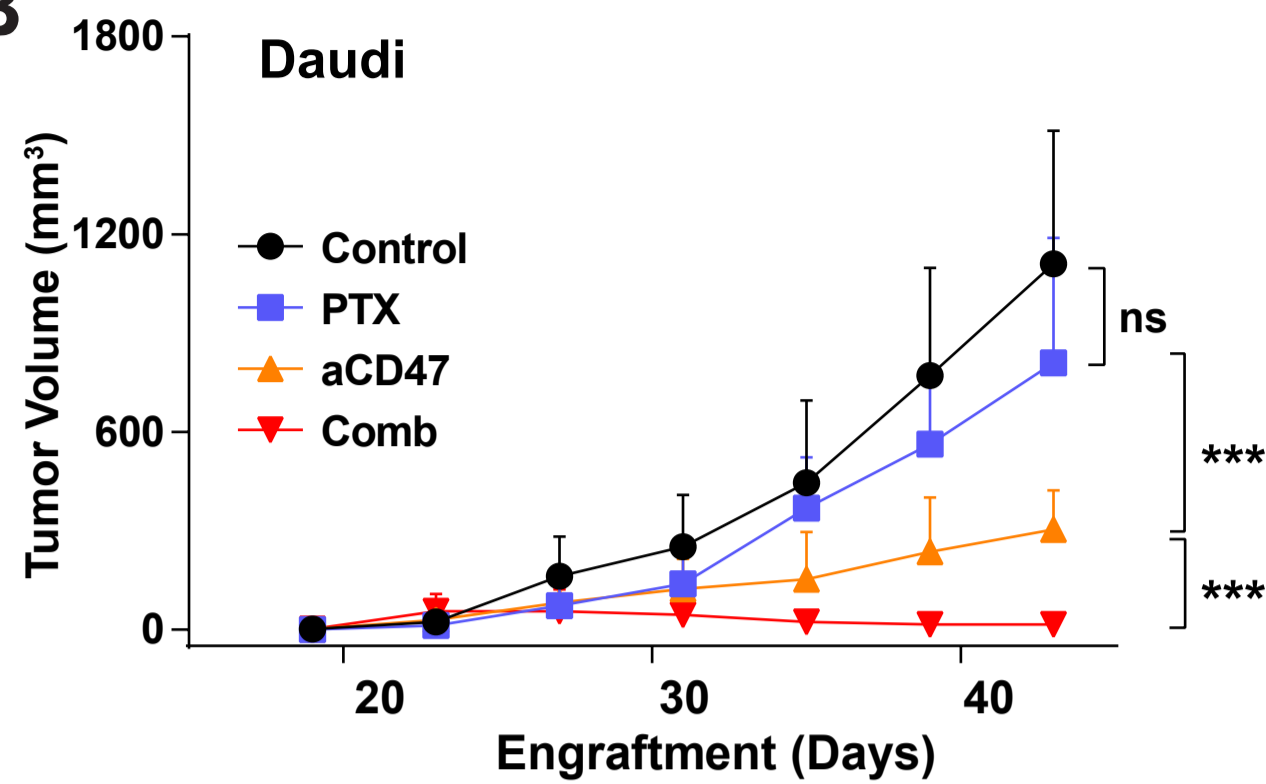


Supplemental Figure 6

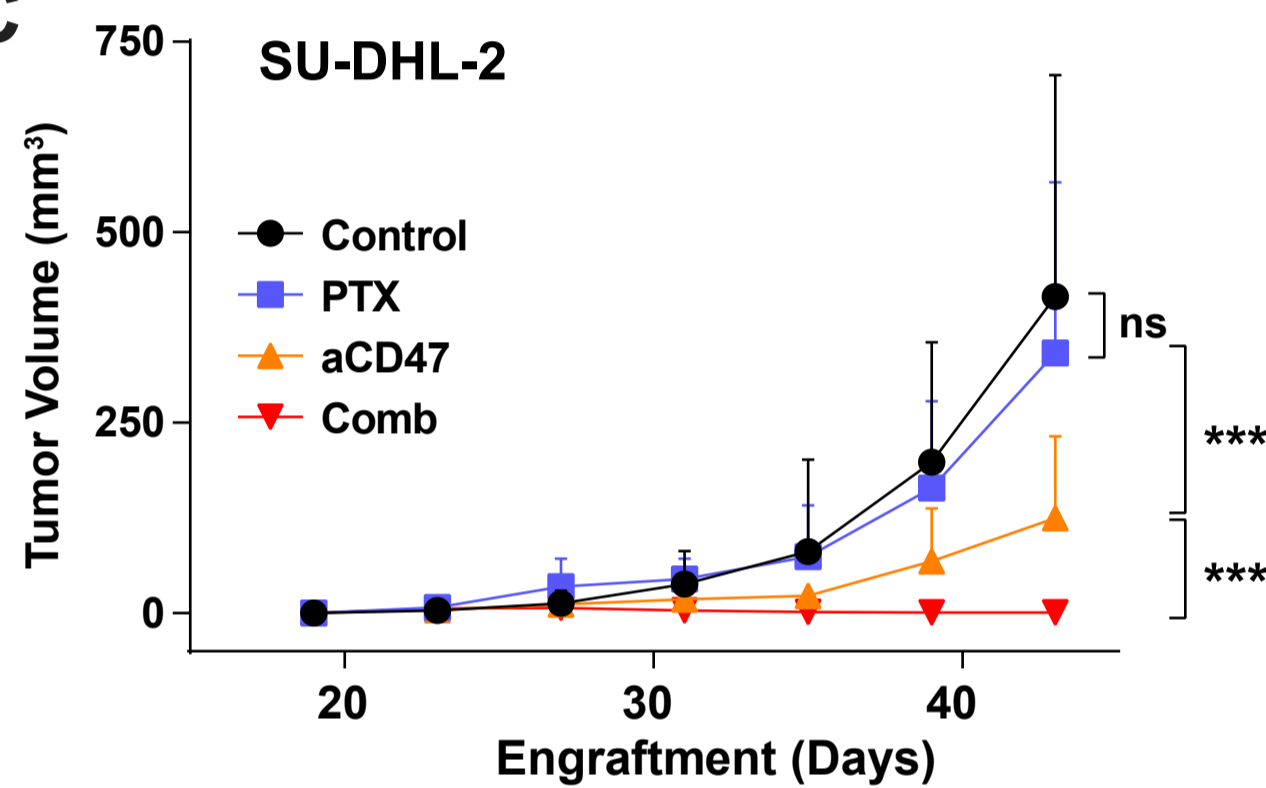
A



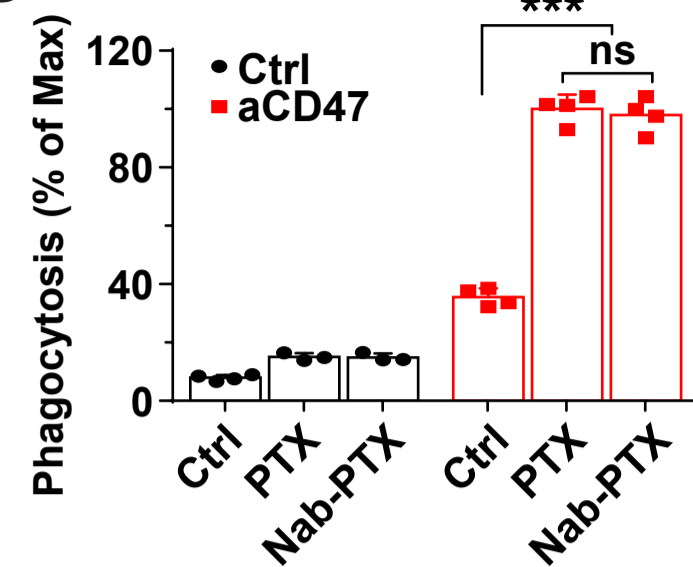
B



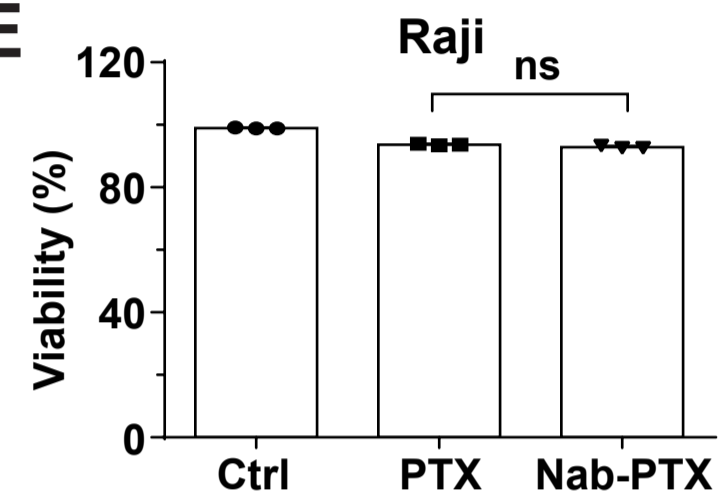
C



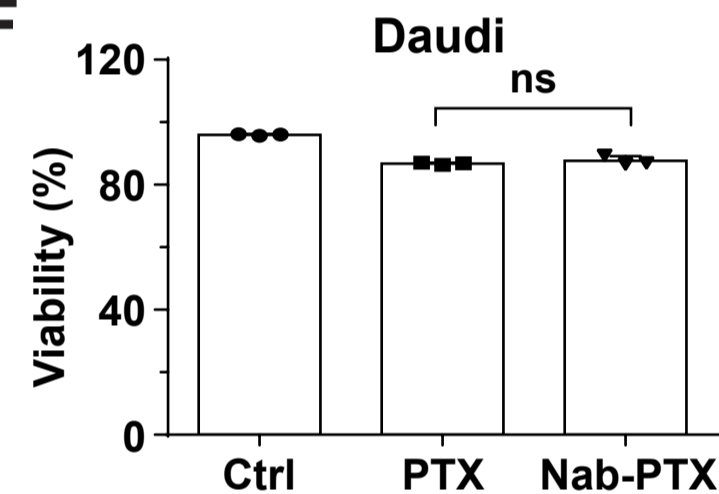
D



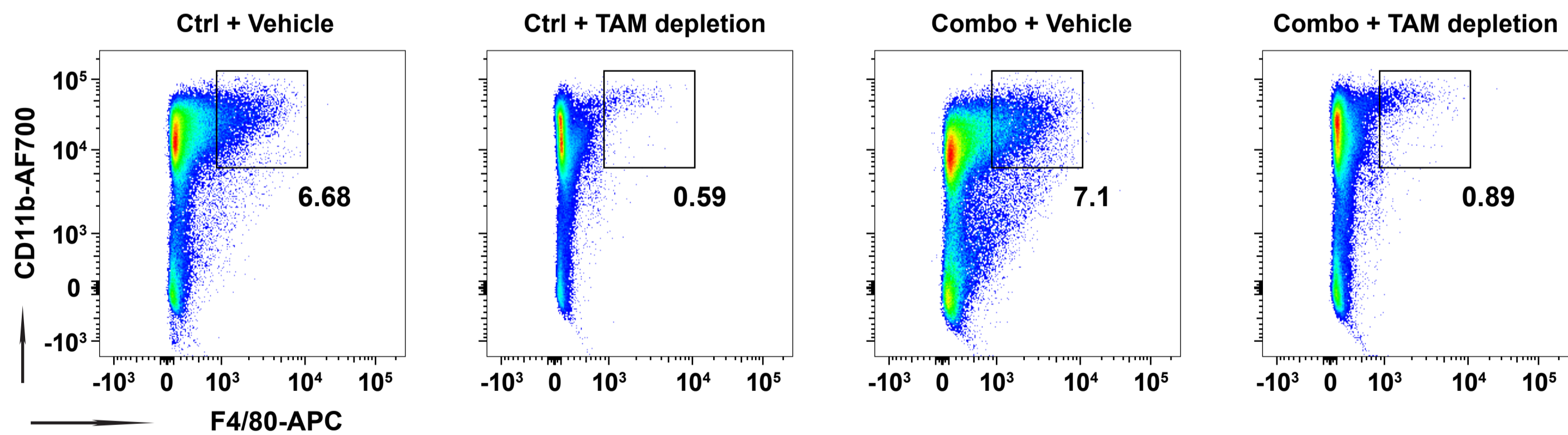
E



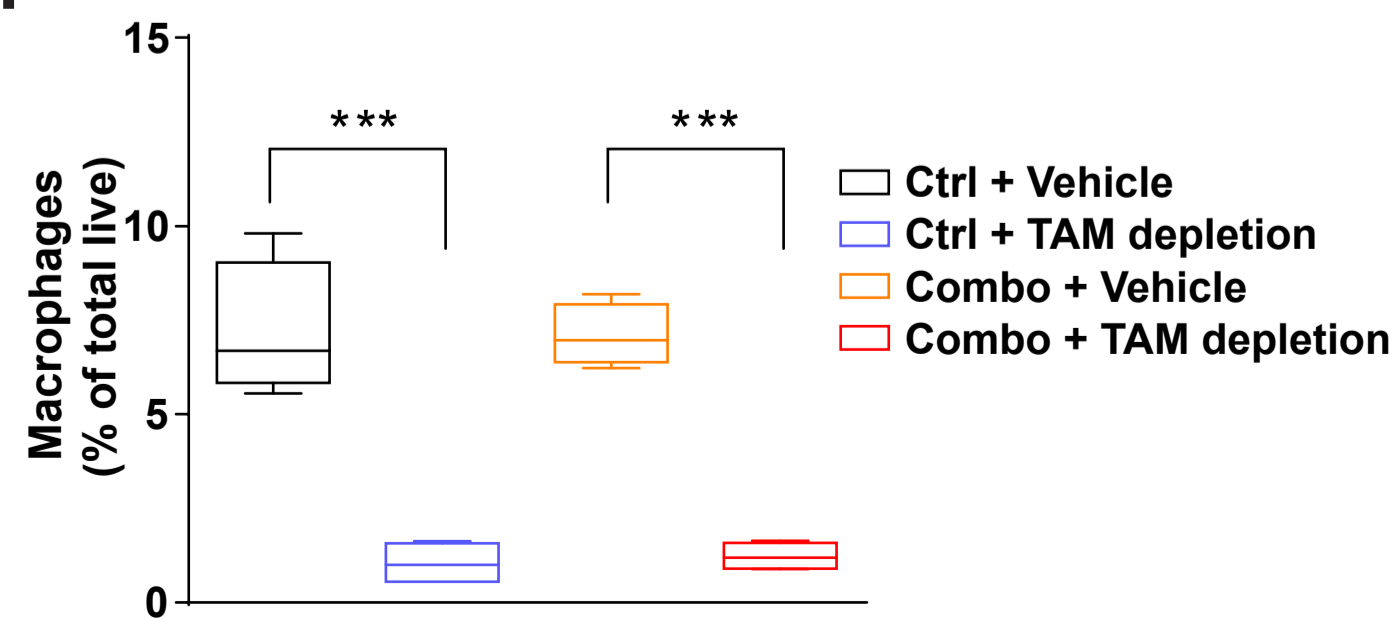
F



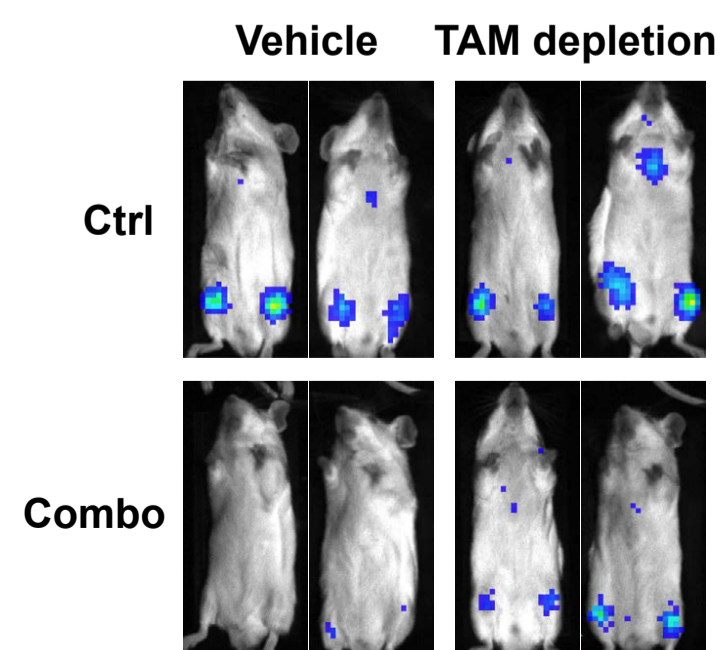
G



H

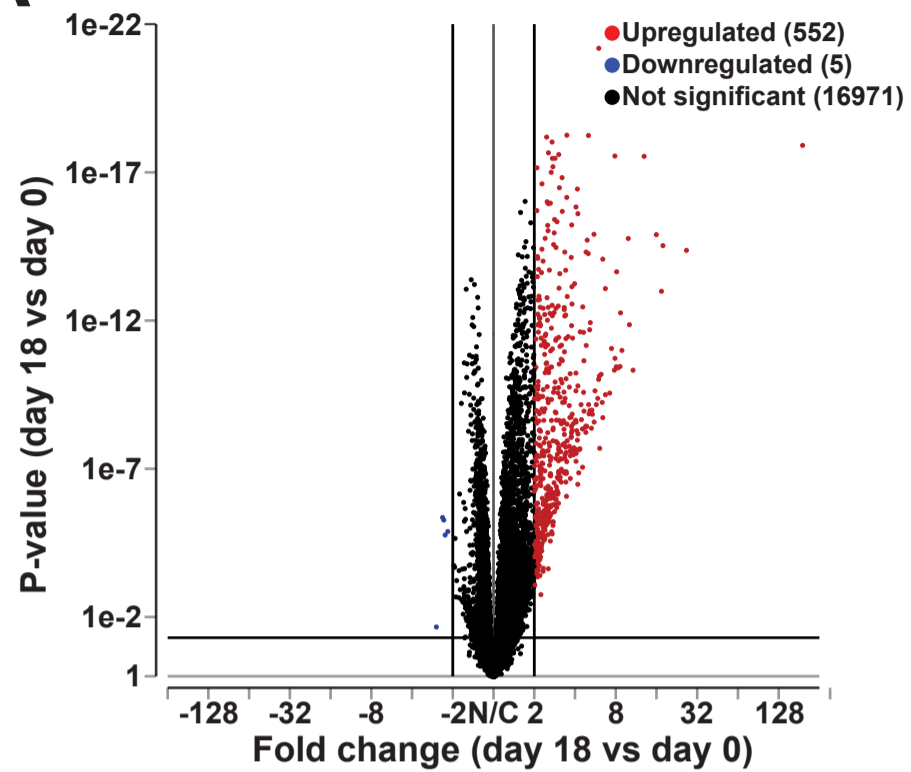


I

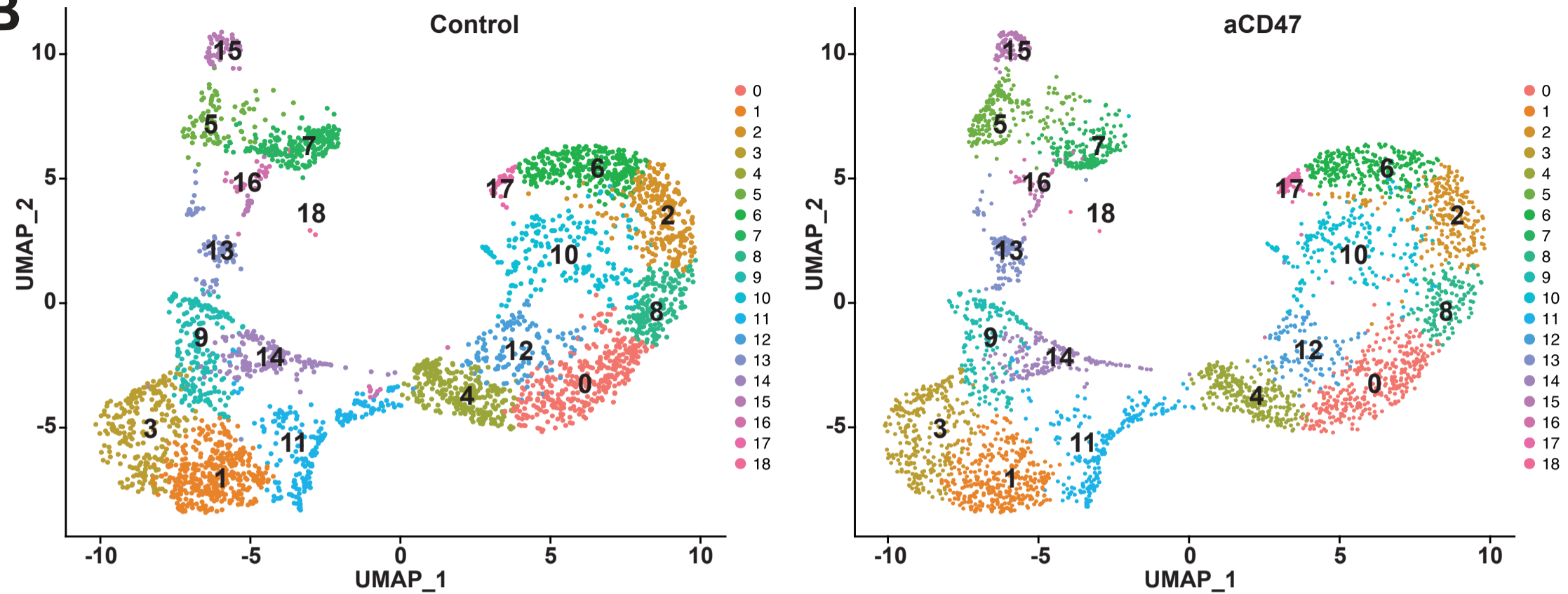


Supplemental Figure 7

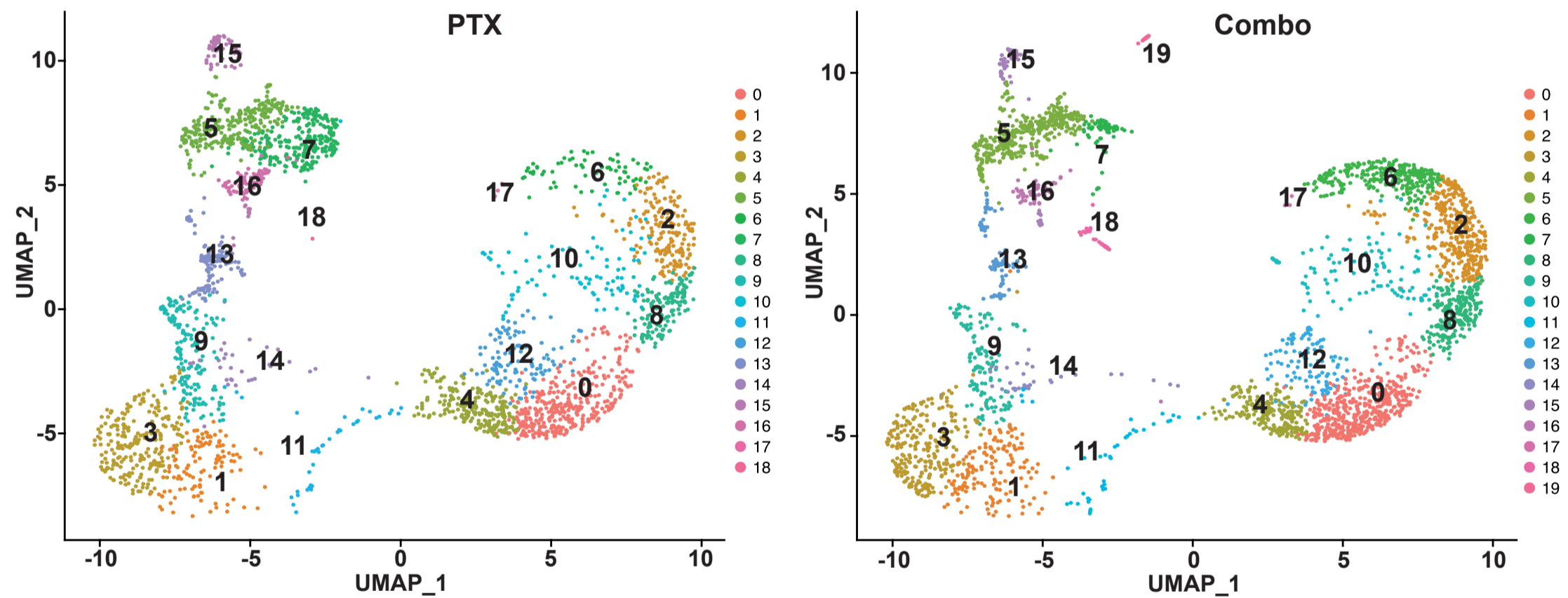
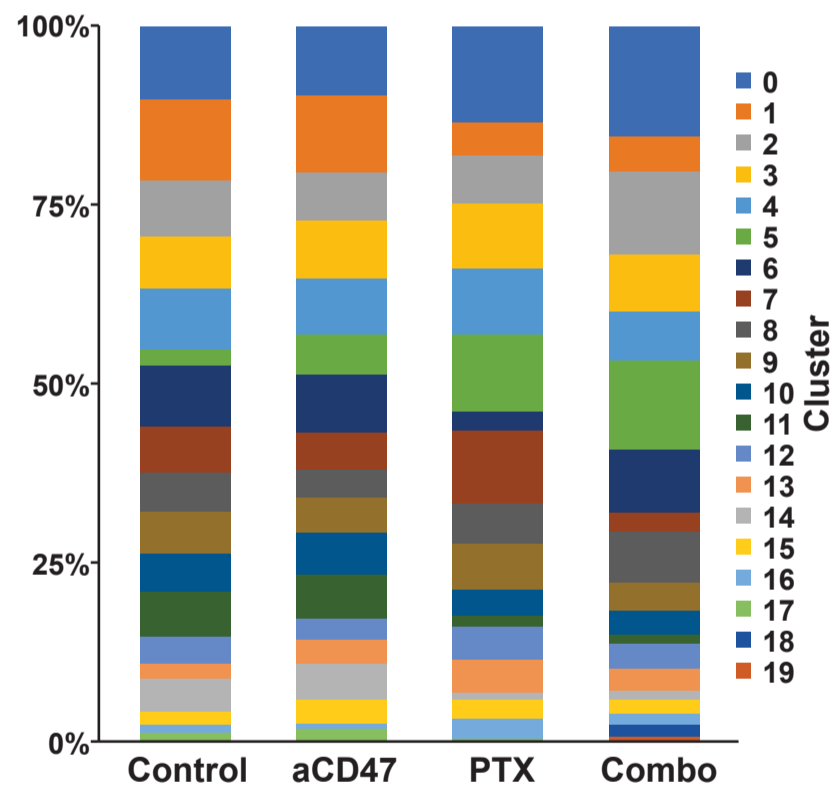
A



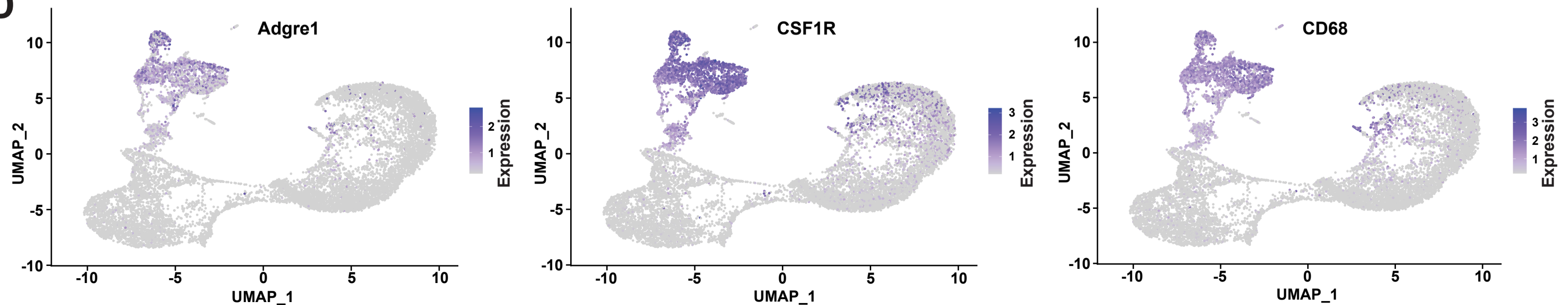
B



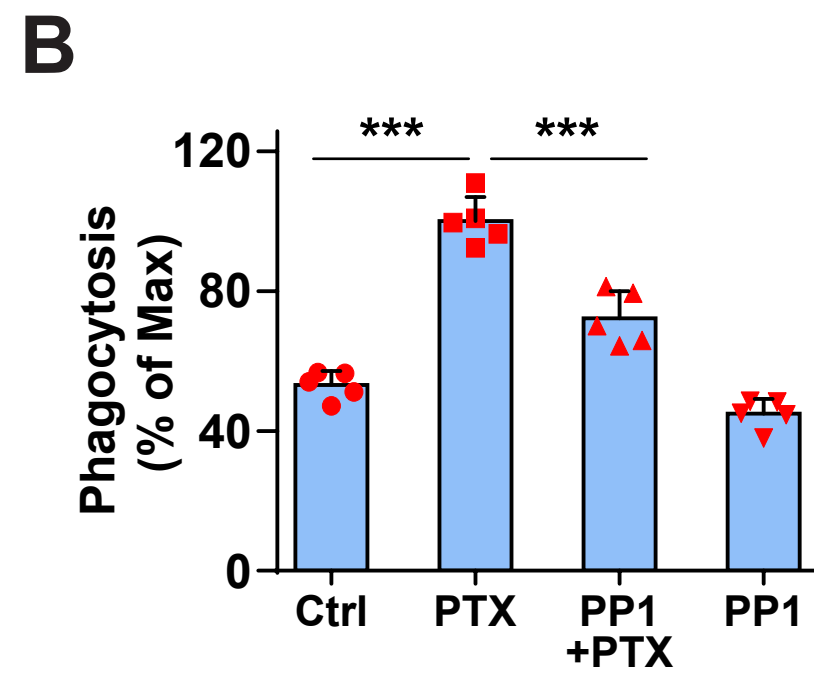
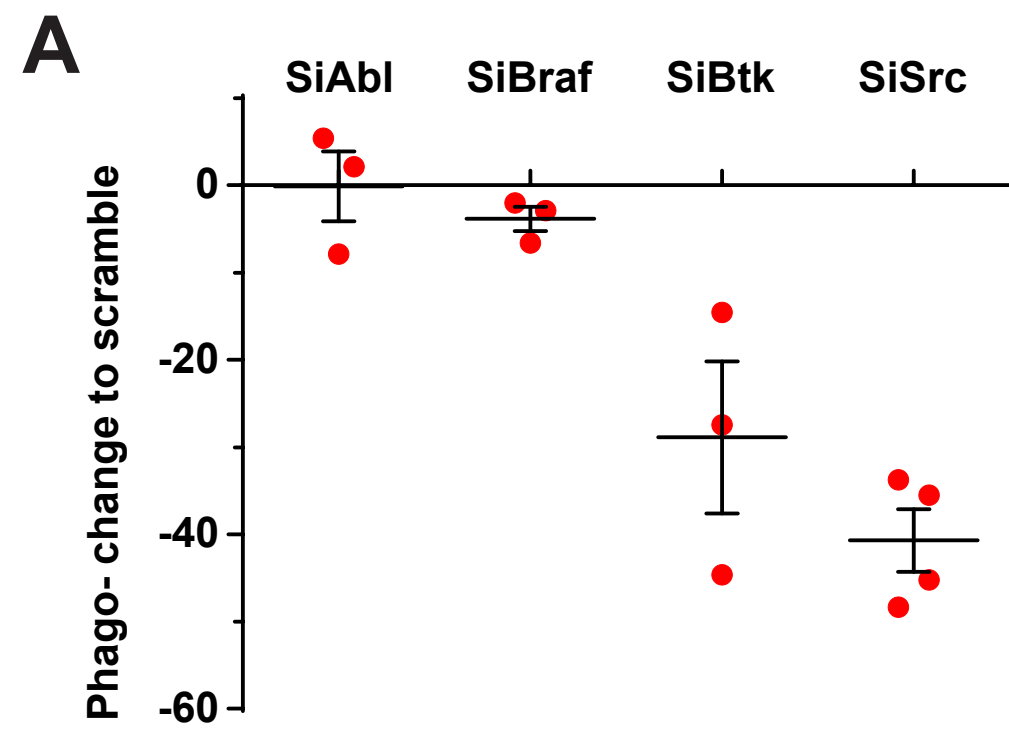
C



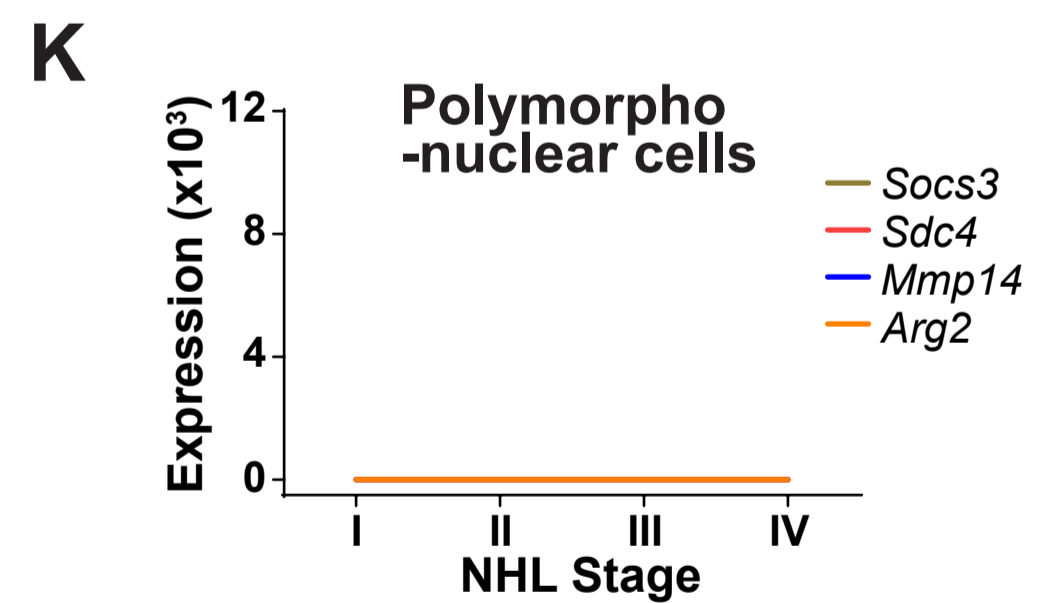
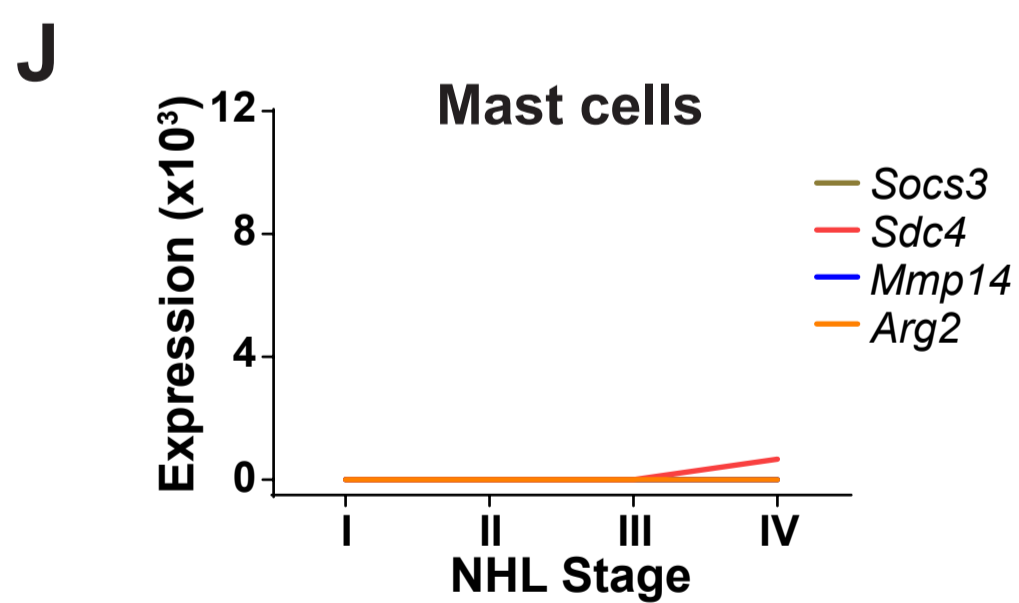
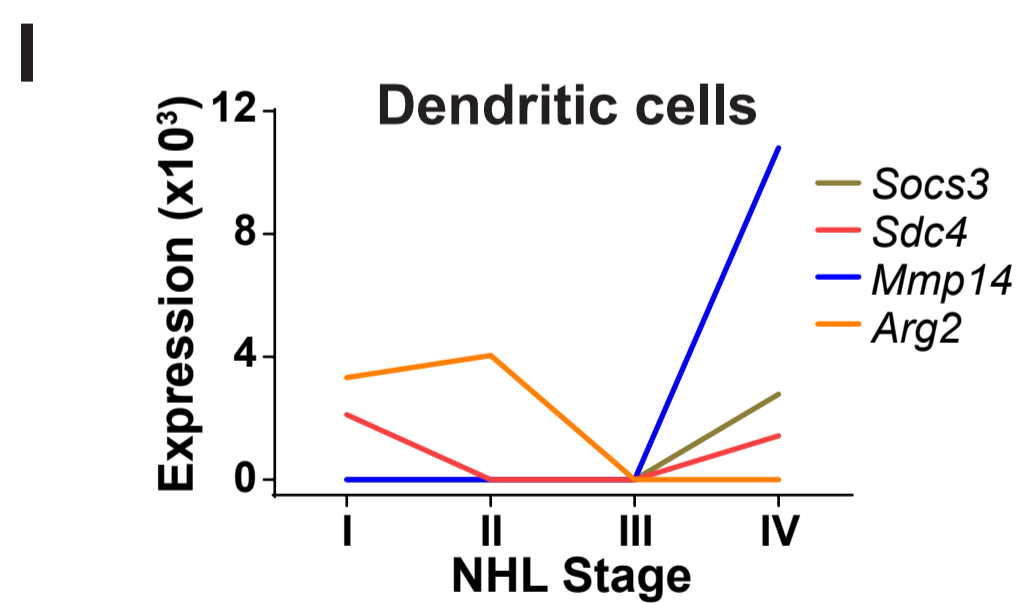
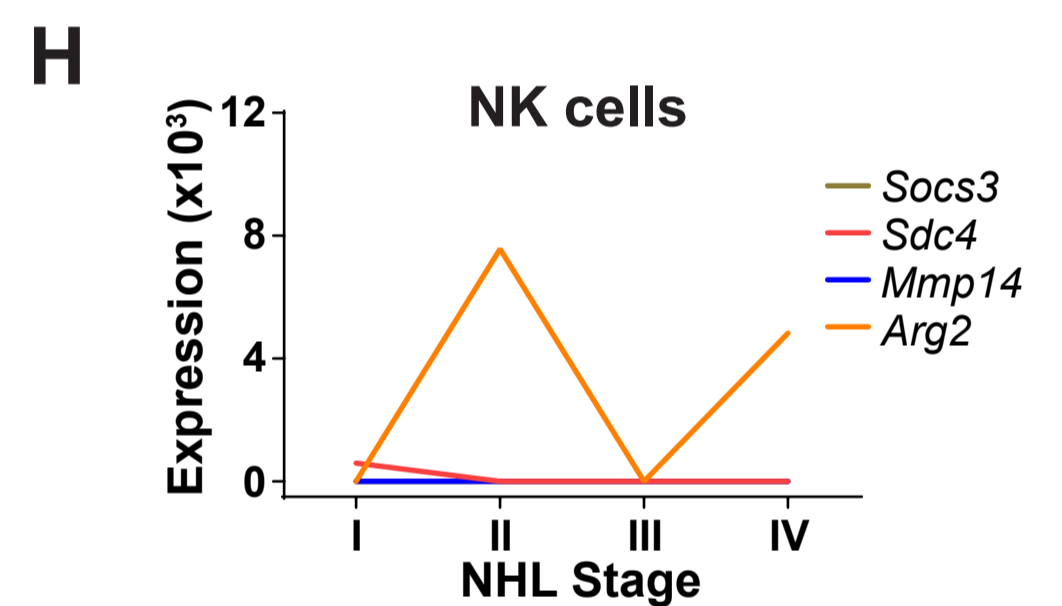
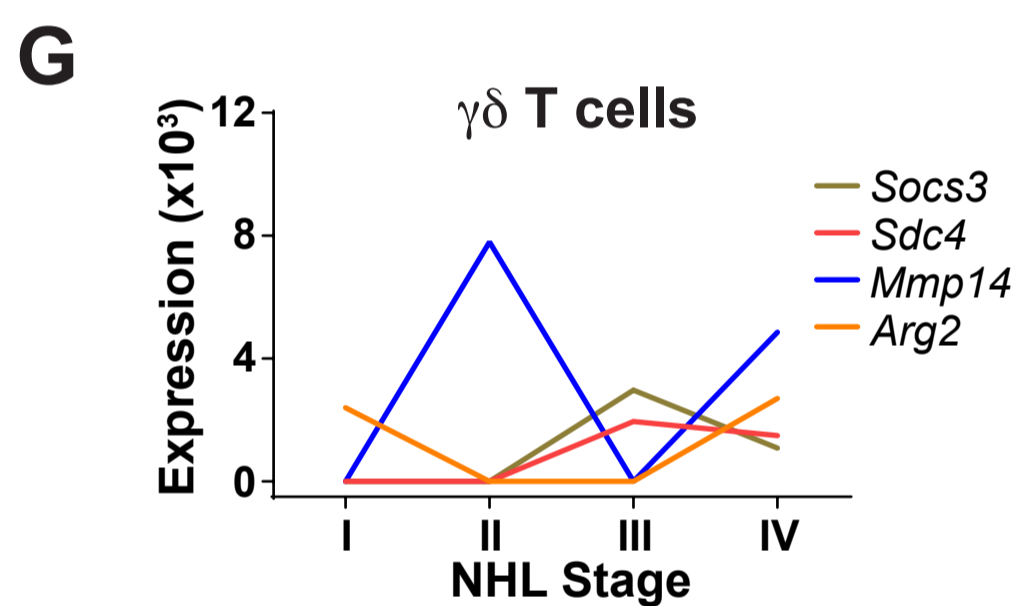
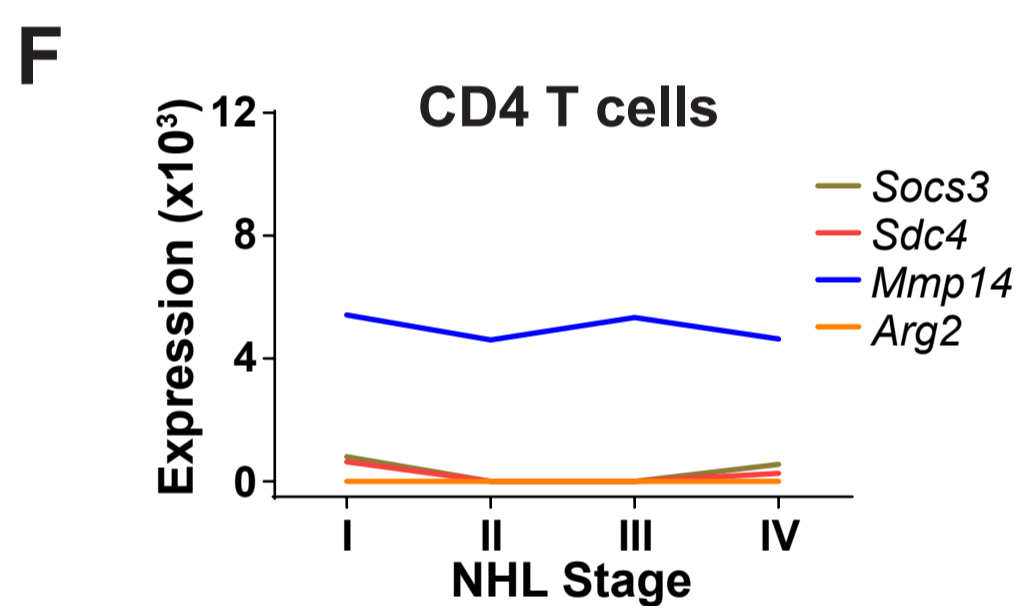
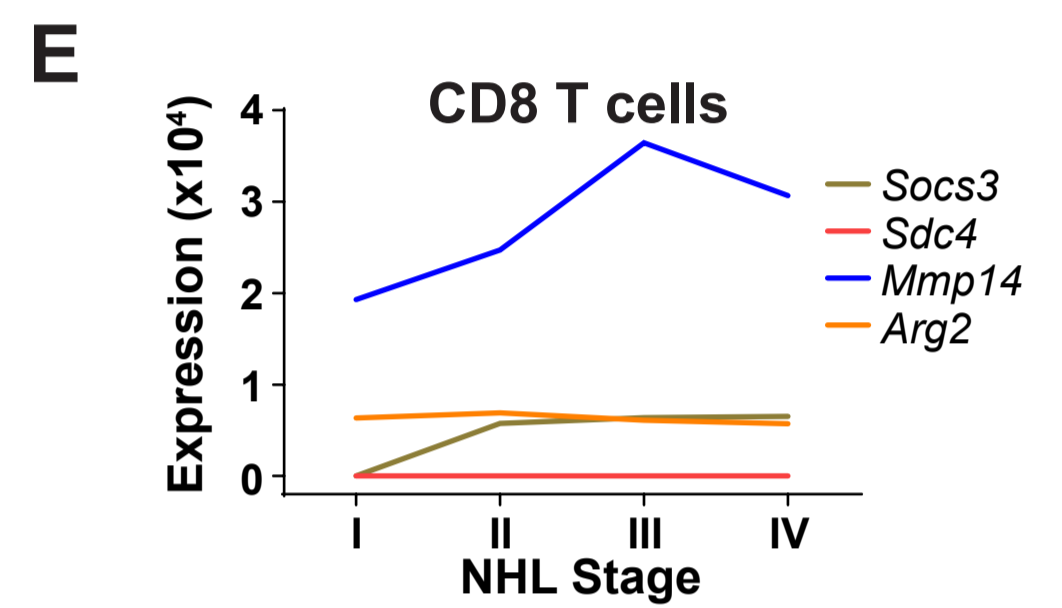
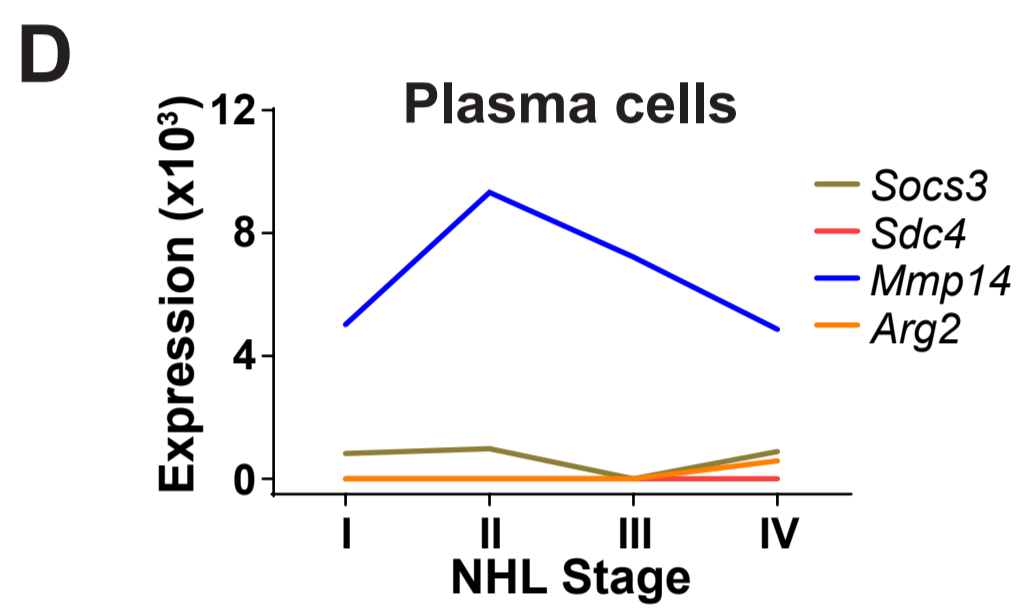
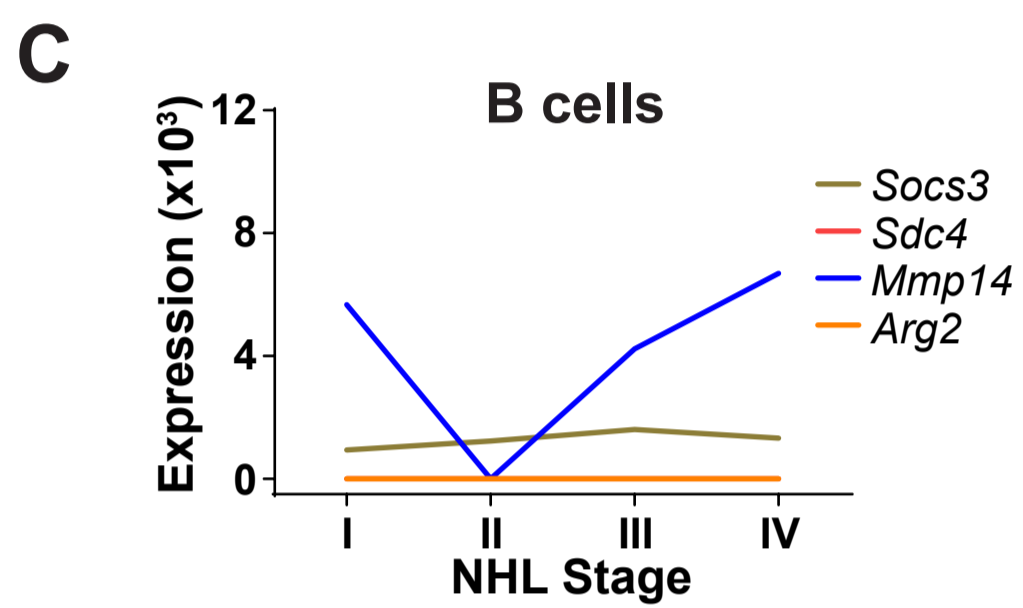
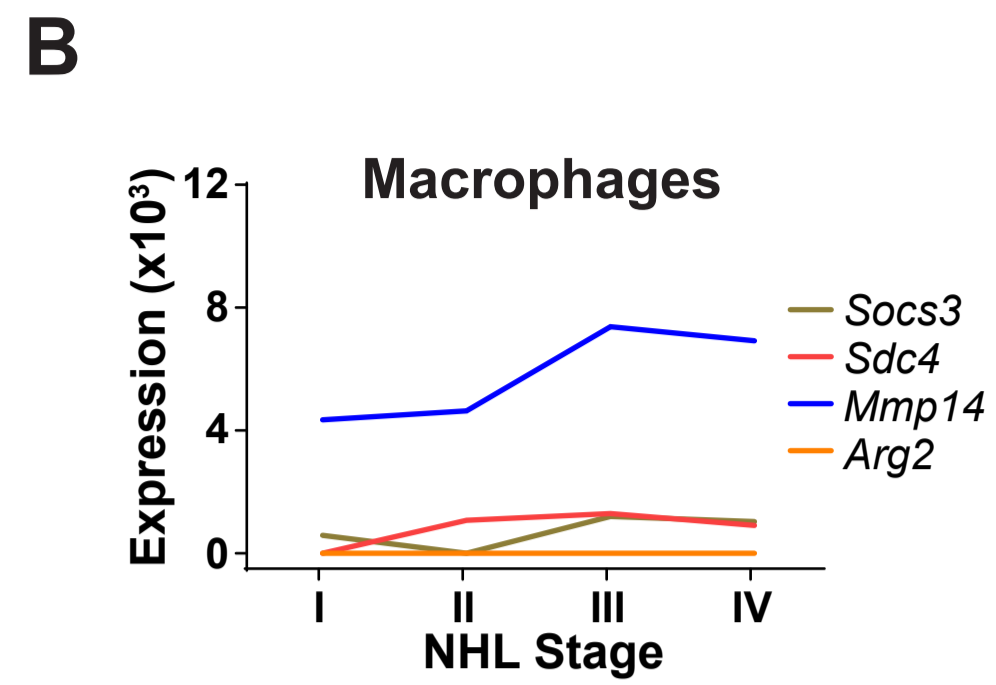
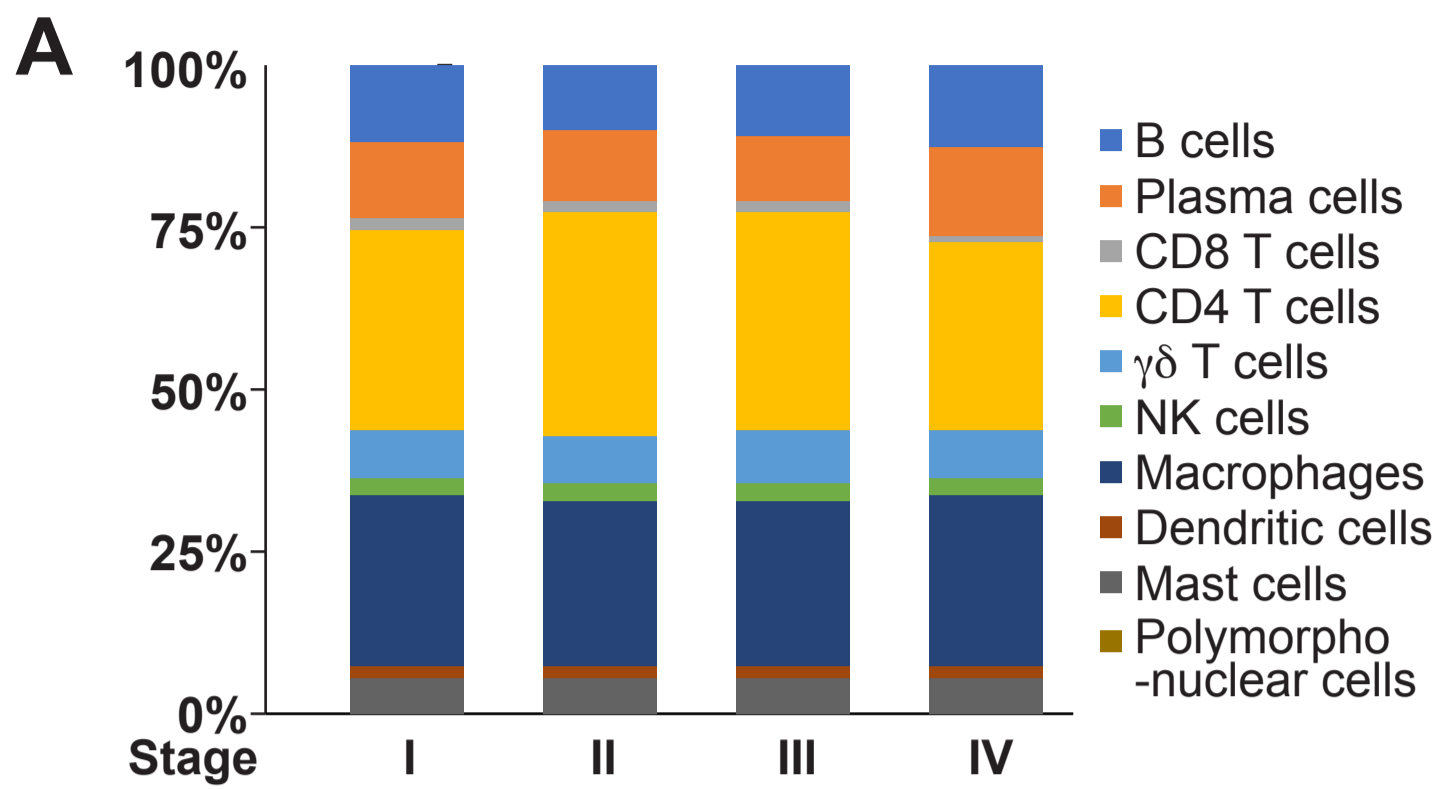
D



Supplemental Figure 8



Supplemental Figure 9



Ifosfamide
Bendamustine hydrochloride
Idarubicin hydrochloride
Carmustine
Dactinomycin
Plicamycin
Dacarbazine
Procarbazine hydrochloride
Cisplatin
Etoposide
Epirubicin hydrochloride
Clofarabine
Estramustine phosphate sodium
Chlorambucil
Pipobroman
Methoxsalen
Lomustine
Dexrazoxane
Oxaliplatin
Vinorelbine tartrate
Capecitabine
Zoledronic acid
Ixabepilone
Cabazitaxel
Nelarabine
Omacetaxine mepesuccinate
Lenalidomide
Plerixafor
Pomalidomide
Uridine triacetate
Enzalutamide
Apalutamide
Abitaterone
Venetoclax
Celecoxib
Tamoxifen citrate
Letrozole
Raloxifene
Anastrozole
Exemestane
Fulvestrant
Pralatrexate
Pemetrexed Disodium salt Heptahydrate
Belinostat
Panobinostat
Vorinostat
Romidepsin
Vismodegib

Erismodegib
Enasidenib
Ivosidenib
Olaparib
Niraparib hydrochloride
Rucaparib phosphate
Talazoparib
Ixazomib citrate
Bortezomib
Carfilzomib
Tretinoin
Gefitinib
Erlotinib hydrochloride
Dasatinib
Pazopanib hydrochloride
Imatinib
Lapatinib
Nilotinib
Sorafenib
Sunitinib
Afatinib
Lenvatinib
Crizotinib
Neratinib
Axitinib
Trametinib
Palbociclib
Ponatinib
Idelalisib
Vandetanib
Cabozantinib
Vemurafenib
Ibrutinib
Regorafenib
Alectinib
Binimetinib
Dabrafenib mesylate
Bosutinib
Dacomitinib
Cobimetinib
Abemaciclib
Duvelisib
Ceritinib
Encorafenib
Ribociclib
Osimertinib
Larotrectinib
Brigatinib

Acalabrutinib
Copanlisib
Sirolimus
Tensirolimus
Everolimus